

Recent developments on nanocomposites based on spinel ferrite and carbon nanotubes for applications in electromagnetic interference shielding and microwave absorption

Raghvendra Singh Yadav & Ivo Kuřitka

To cite this article: Raghvendra Singh Yadav & Ivo Kuřitka (2023): Recent developments on nanocomposites based on spinel ferrite and carbon nanotubes for applications in electromagnetic interference shielding and microwave absorption, Critical Reviews in Solid State and Materials Sciences, DOI: [10.1080/10408436.2023.2214577](https://doi.org/10.1080/10408436.2023.2214577)

To link to this article: <https://doi.org/10.1080/10408436.2023.2214577>



© 2023 The Author(s). Published with license by Taylor & Francis Group, LLC



Published online: 02 Jun 2023.



Submit your article to this journal [↗](#)



Article views: 117





View related articles [↗](#)



View Crossmark data [↗](#)

Recent developments on nanocomposites based on spinel ferrite and carbon nanotubes for applications in electromagnetic interference shielding and microwave absorption

Raghvendra Singh Yadav  and Ivo Kuřitka 

Centre of Polymer Systems, University Institute, Tomas Bata University in Zlín, Trida Tomase Bati, Zlín, Czech Republic

ABSTRACT


Several carbon nanotubes and spinel ferrite-based nanocomposites have been created in recent years and are considered to be viable options for an effective electromagnetic interference (EMI) shielding and microwave absorber material. The current development of carbon nanotube and spinel ferrite-based nanocomposites for EMI shielding and microwave absorption is the topic of this study. The fundamental mechanism of EMI shielding and microwave absorption is described. The EMI shielding and microwave absorption properties of carbon nanotubes and spinel ferrite, as well as their numerous components such as graphene, MXene, semiconductor nanoparticles, polymer, rubber, and so on, are thoroughly examined. This paper also discusses potential problems and solutions for creating new nanocomposites for the next generation of shielding applications.

KEYWORDS

Carbon nanotubes; spinel ferrite; electromagnetic interference shielding; microwave absorption

Table of contents

1. Introduction	2
2. The basic theory of EMI shielding and microwave absorption	4
2.1. EMI shielding effectiveness	4
2.2. Microwave absorption	5
2.3. Influencing factors on EMI shielding and microwave absorption characteristics	5
2.3.1. Dielectric loss	5
2.3.2. Magnetic loss	6
2.3.3. Skin depth	6
2.3.4. Impedance matching	6
2.3.5. Attenuation constant	6
2.3.6. Another factor	7
3. Carbon nanotube and spinel ferrite based nanocomposites	7
3.1. Carbon nanotube and Fe ₃ O ₄ based nanocomposites	7
3.2. Carbon nanotube and CoFe ₂ O ₄ based nanocomposites	10
3.3. Carbon nanotube and NiFe ₂ O ₄ based nanocomposites	12
3.4. Carbon nanotube and mixed spinel ferrite based nanocomposites	12
4. Graphene, carbon nanotube, and spinel ferrite based nanocomposites	14
5. Carbon, carbon nanotube, and spinel ferrite based nanocomposites	16
6. MXene, carbon nanotube and spinel ferrite based nanocomposites	17
7. Doped carbon nanotubes and spinel ferrite based nanocomposites	19
8. Coated carbon nanotubes and spinel ferrite based nanocomposites	21
9. Polymer, carbon nanotube, and spinel ferrite based nanocomposites	24
10. Semiconducting nanoparticles, carbon nanotubes, and spinel ferrite based nanocomposites	27
11. Rubber, carbon nanotubes, and spinel ferrite based nanocomposites	29

CONTACT Raghvendra Singh Yadav  yadav@utb.cz

© 2023 The Author(s). Published with license by Taylor & Francis Group, LLC

This is an Open Access article distributed under the terms of the Creative Commons Attribution-NonCommercial-NoDerivatives License (<http://creativecommons.org/licenses/by-nc-nd/4.0/>), which permits non-commercial re-use, distribution, and reproduction in any medium, provided the original work is properly cited, and is not altered, transformed, or built upon in any way. The terms on which this article has been published allow the posting of the Accepted Manuscript in a repository by the author(s) or with their consent.

12. Conclusion and perspective	31
Acknowledgment	32
Disclosure statement	32
References	32

1. Introduction

Nowadays, widespread use of mobile communication devices and electronic equipment, which emit electromagnetic (EM) waves as a byproduct, raises the possibility of EM radiation pollution (Figure 1).^[1–5] Electromagnetic (EM) waves cause signal distortion, malfunction of electrical equipment, and harm to human health.^[6,7] Various electromagnetic interference (EMI) shielding materials have been developed to mitigate or limit the harm caused by EM wave pollution.^[8,9] The mechanism of EMI shielding materials was generally comprised of reflection, absorption, and multiple reflections.^[10] Traditional shielding materials, such as metals, have been employed as shielding materials because to their high conductivity; however, metals have a high density, are prone to corrosion, and are difficult to handle.^[11] Furthermore, EM radiation is not completely decreased since EM waves are reflected from the metal surface and interact with surrounding electronics, causing additional interference.^[12] The approach to filter out harmful EM radiation is absorption shielding.^[13] Impedance matching and EM energy attenuation are essential considerations in the creation

of high-performance EM wave absorber materials.^[14] The relative complex permeability, relative complex permittivity, EM impedance matching, component, and structure of the EMI shielding material influence the reflection and attenuation of EM waves.^[15] The incident EM waves are strongly absorbed in green EMI shielding material, preventing reflections and transmissions and maximizing shielding effectiveness while minimizing secondary EM pollution.^[16] Magnetic materials are frequently added to enhance impedance matching and adjust multiple attenuation in order to achieve green shielding. A multi-component composite with magnetic-dielectric synergy exhibits effective green EMI shielding and excellent microwave absorption.^[17]

Carbon-based materials with varied structures and phases are the most promising candidates for electrically conductive materials due to their low density, plentiful resources, strong electrical properties, ease of synthesis, and high chemical and thermal stabilities.^[18–21] Carbon materials, especially carbon nanotubes (CNTs), have attracted increased attention in recent years for their high-performance electromagnetic wave absorption qualities because to their lightweight, high aspect ratio, remarkable mechanical



Figure 1. Schematic illustration of an intelligent world, including wearable devices, intelligent bodies, and autonomous vehicles. EM absorption materials are a bridge connecting the micro and macro world. Reproduced with permission from Ref. [3]. Copyright 2022. Elsevier Publication.

strength, and high electrical conductivity.^[22–25] Suman Kumar Ghosh et al.^[26] reported carbon nanotubes and carbon nanofibers based co-continuous thermo-plastic elastomeric blend composites and noticed EMI shielding performance of -36.7 dB for 15 wt% of nanofiber loading. Palash Das et al.^[27] reported a self-healable and super-stretchable conductive elastomeric nanocomposite and noticed that the nanocomposite with MWCNTs (15 phr) exhibited an excellent EMI shielding effectiveness of -27.4 dB. G. Sang et al.,^[28] demonstrated effective electromagnetic interference shielding of nickel@multiwalled carbon nanotubes/alumina composites. The high-performance EM absorption feature linked with the innovative structure and the double losses of magnetic Co and dielectric CNTs was reported by Xiangyun Xiao et al.^[29] When Ming-Ming Lu et al.^[30] created a multiscale assembly of carbon nanotubes and grape-like ferroferric oxide, they discovered that the unique combination of MWCNTs and magnetic loss nanocrystals offered a practical method for realizing excellent absorbers at high temperatures. In a layered structure of carbon foam coated with carbon nanotubes and a FeNi alloy, Yangjun Zou et al.^[31] found the best reflection loss to be -64 dB with an effective absorption bandwidth (EAB) of 7.4 GHz. Due to synergistic magnetic-dielectric effects, unique structural merits, and heterostructure tailoring of carbon nanotubes grown on prismatic NiCo clusters, Jiajun Xu et al.^[32] reported remarkable EM absorption performance with a minimum reflection loss of -46.2 dB at 1.5 mm and broad bandwidth of 5.8 GHz. Longqi Yang et al.^[33] created a multi-dimensional NiCo/C/CNT/rGO aerogel using a metal-organic framework (MOF) derivative, and at a filler loading of 20 weight percent, with a thickness of 1.8 mm and an effective absorption bandwidth of 7.6 GHz, they achieved the best electromagnetic wave absorption performance of -58.8 dB. Jiana Hu et al.^[34] created a double-layered MXene-Fe/carbon nanotube/silicone rubber composite and recorded a reflection loss value of -65.9 dB at 12 GHz and an effective absorption bandwidth up to 8.24 GHz at 2.86 mm thickness. CuCo nanocube/N-doped carbon nanotube composites were created by Zhiqian Yao et al.,^[35] and noticed that at an annealing temperature of 850°C , the minimum reflection loss (RL_{\min}) of CuCo/NCNT could reach 54.13 dB with an effective absorption bandwidth of 4.01 GHz.

Metal oxides known as spinel ferrites have a spinel structure with the general formula AB_2O_4 , where A and B are metallic cations located at two different crystallographic sites, tetrahedral (A site) and

octahedral (B site), respectively.^[36] Both positions' cations are octahedrally and tetrahedrally coordinated to oxygen atoms, respectively. Iron (III) must be present in the chemical formula for the substances to be called ferrite, at least. MFe_2O_4 is a common example of a ferrite, where M stands for Mn, Fe, Co, Ni, Cu, and Zn. There are 64 tetrahedral and 32 octahedral positions available for cations in a single unit cell of ferrite, but only 8 tetrahedral and 24 octahedral positions are occupied by cations. Depending on their affinity for both positions, the distributions of each metal cation over both sites vary, which is dependent on the conditions used during the synthesis time, the types of synthesis, the ionic radii of the cations, the size of the interstices, and the stabilization energy. A normal spinel structure results from completely occupying the tetrahedral site with a divalent transition metal, whereas an inverse spinel structure results from completely occupying the octahedral site with the divalent transition metal ions. The structure is mixed or disordered if divalent transition metal ions are present on both the A and B sub-lattices. Due to their useful optical behavior, improved mechanical strength, enhanced diffusivity and suitable specific heat, high electrical and high magnetic properties, spinel ferrite nanoparticles with a high surface to volume ratio have drawn a lot of interest.^[37]

Spinel ferrites have been identified as a possible contender within the range of EM wave absorber magnetic materials owing to their abundant raw material, cheap cost, high dispersibility, environmental benignity, nontoxicity, and remarkable electromagnetic properties.^[38] However, because of the low impedance matching requirements, these single-phase spinel ferrite magnetic materials have the disadvantages of having a limited absorption bandwidth, requiring a high thickness, and being dense, limiting their practical utility as an EMI shielding material. As a result, combining additional electrically conductive materials to create multiphase composite spinel ferrite magnetic materials may be an effective technique for achieving excellent EM wave absorption. The increased permittivity of conductive material combined with the low dielectric value of spinel ferrite magnetic material will result in a sufficient permittivity value, which necessitates a better impedance matching level.^[39] This study will concentrate on the most recent advancements in the EM wave absorption application accomplished by carbon nanotubes and spinel ferrites, as shown in Figure 2. This is the first review of carbon nanotube and spinel ferrite-based

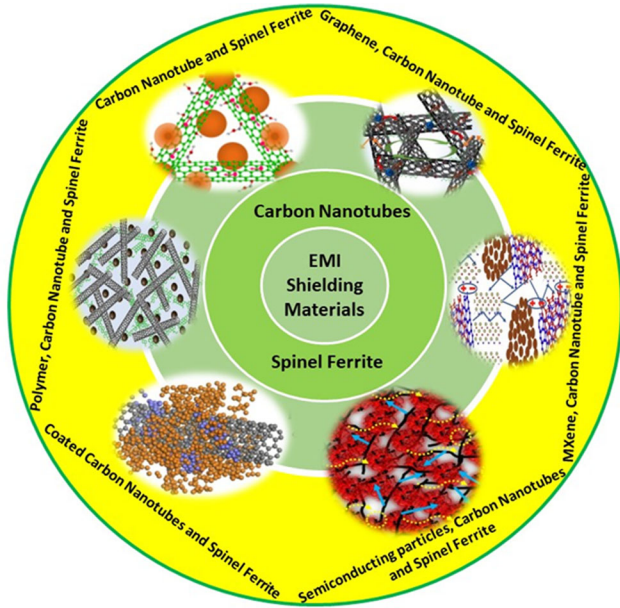


Figure 2. Schematic illustration of carbon nanotubes and spinel ferrite-based nanocomposites for electromagnetic interference shielding applications. Reproduced with permission from Ref. [74]. Copyright 2022. Elsevier Publication. Reproduced with permission from Ref. [90]. Copyright 2022. Elsevier Publication. Reproduced with permission from Ref. [95]. Copyright 2022. Elsevier Publication. Reproduced with permission from Ref. [113]. Copyright 2019, ACS Publication. Reproduced with permission from Ref. [102]. Copyright 2022. Elsevier Publication. Reproduced with permission from Ref. [110]. Copyright 2021, RSC Publication.

nanocomposites for EMI shielding and microwave absorption.

2. The basic theory of EMI shielding and microwave absorption

2.1. EMI shielding effectiveness

The material's total EMI shielding effectiveness (SE_T) is stated as the ratio of incoming EM radiation power to transmitted radiated power^[40]:

$$SE_T = 10 \log \left(\frac{P_{in}}{P_t} \right) = 20 \log \left(\frac{E_{in}}{E_t} \right) = 20 \log \left(\frac{H_{in}}{H_t} \right)$$

where P_{in} , E_{in} , and H_{in} indicate incident power, electric field intensities, and magnetic field intensities on the shielding materials, respectively; whereas, P_t , E_t , and H_t represent transmitted power, electric field intensities, and magnetic field intensities, respectively. The frequency dependence of SE_T is investigated. A high SE_T value indicates that less energy passes through the shielding material. The overall EMI shielding efficacy is characterized by the following relation^[41] according to Schelkunoff's theory:

$$SE_T = SE_R + SE_A + SE_M$$

Surface reflection, internal absorption, and multiple interior reflections are denoted as SE_R , SE_A , and SE_M , respectively. SE_R is the contribution from the impedance mismatch between the incident EM wave and the shield's surface impedance. Furthermore, the reflection of an incoming EM wave is related to the surface charge in the shielding material, which requires the shielding material to be electrically conducting in nature.^[42] It is also worth mentioning that SE_A is related with high electrical conductivity for shielding material ohmic loss, dielectric loss, and magnetic loss. Surprisingly, the impact of SE_M may be avoided when the shield thickness is close to or more than the skin depth, or when the SE_T is greater than 10 dB.^[43]

The reflection and transmission coefficient, as well as the overall shielding effectiveness (SE_T), can be typically evaluated using the scattering parameters S_{11} , S_{22} , S_{12} , and S_{21} that can be obtained from the Vector analyzer. Here, S_{11} , S_{12} , and S_{21} stand for the forward reflection coefficient, reverse transmission coefficient, and forward transmission coefficient, respectively. The following equations can be used to determine the transmission coefficient (T), reflection coefficient (R), and absorption coefficient (A) of electromagnetic waves^[44]:

$$T = |S_{12}|^2 = |S_{21}|^2$$

$$R = |S_{11}|^2 = |S_{22}|^2$$

$$A = 1 - R - T$$

SE_T can be evaluated by the following relation:

$$SE_T (dB) = 10 \log \frac{1}{T} = 10 \log \frac{1}{|S_{12}|^2} = 10 \log \frac{2}{|S_{21}|^2}$$

Following equations can be utilized to evaluate SE_A (absorption) and SE_R (reflection) parameters:

$$SE_A (dB) = 10 \log \left[\frac{1}{1 - A_{eff}} \right] = 10 \log \left[\frac{1 - R}{T} \right]$$

$$= 10 \log \left[\frac{1 - S_{11}^2}{S_{11}^2} \right]$$

$$SE_R (dB) = 10 \log \left[\frac{1}{1 - R} \right] = 10 \log \left[\frac{1}{1 - S_{11}^2} \right]$$

The first interaction that takes place at the surface of a conductive shielding material when EM waves strike, it is reflection. Strong EM wave reflection is caused by the impedance mismatch between the shield's conductive surface and the air; consequently,

the more electrically conductive the shield is, the more electrons there are near the surface, increasing the EM wave reflection. The SE_R value can be evaluated as^[45]:

$$SE_R(dB) = 39.5 + 10 \log \frac{\sigma}{2\pi f \mu}$$

where μ and σ are the magnetic permeability and electrical conductivity of the shielding material, respectively; and f is the frequency of the incident EM Waves. According to this equation, the reflection-based shielding is enhanced by greater electrical conductivity or decreased magnetic permeability.

Some EM waves can pass through the shield's surface and propagate its interior after impact. As a function of penetration depth, waves that are propagating are exponentially attenuated. The conducting, dielectric, and magnetic characteristics of the shield are responsible for the attenuation (absorption loss), and an attenuation constant (α) value is given as^[45]:

$$\alpha = \omega \sqrt{\frac{\mu \varepsilon}{2} \left[\sqrt{1 + \left(\frac{\sigma}{\omega \varepsilon} \right)^2} - 1 \right]}$$

where ω is angular frequency, μ is magnetic permeability, ε is dielectric permittivity and σ is electrical conductivity. The outstanding absorption loss is generally attributed to high μ , ε , and σ values, which refers higher magnetic, dielectric and conductance losses. It's crucial to note that while a higher electrical conductivity value reduces the absorption ratio, however, it will increase the effectiveness of the absorption through eddy current or conductance loss. The SE_A value can be estimated as^[45]:

$$SE_A(dB) = 8.68 t \sqrt{\pi f \mu \sigma}$$

here t denotes thickness. The equation tells us that conductivity, sample thickness, and material permeability are the three main variables that affect absorption loss.

2.2. Microwave absorption

In general, the reflection loss (RL) is used to compute the material's microwave absorption characteristic. Based on transmission line theory,^[46] it may be assessed as follows:

$$RL = 20 \log \frac{|Z_{in} - Z_o|}{|Z_{in} + Z_o|}$$

$$Z_{in} = Z_o \sqrt{\mu_r / \varepsilon_r} \tanh \left[j(2\pi f d / c) \sqrt{\varepsilon_r / \mu_r} \right]$$

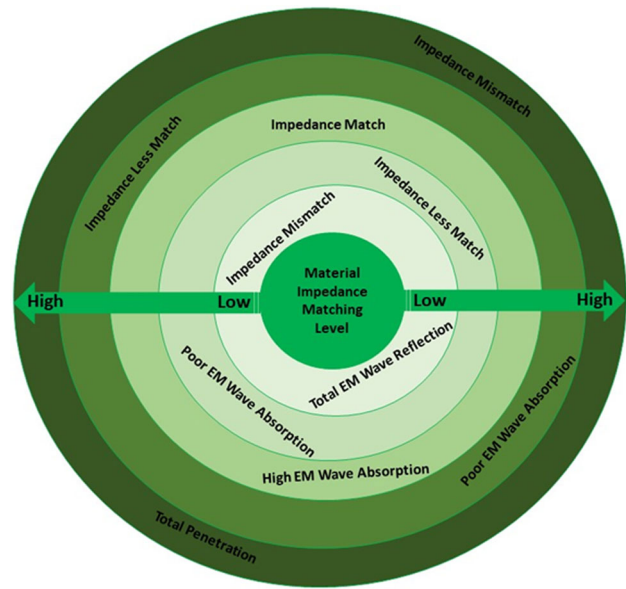


Figure 3. Dependence of EM Wave Absorption Characteristics on Impedance Matching.

where c , f , d , Z_{in} , and Z_o are the light velocity, frequency, absorbing material thickness, input impedance, and free space impedance (377), respectively. The aforementioned relationships explain that if a microwave absorption material is produced with an input impedance equal to that of free space, there will be no reflection at the material's surface, implying that all incoming EM waves will transmit into the material. It's called impedance matching.^[47] However, in the $Z_{in} \approx Z_o$ condition, the transmission coefficient is unity, indicating that the incident EM wave will transmit out without any dissipation from the material's back surface.^[48] As a result, not only are the essential impedance matching conditions needed, but also strong EM wave absorption by the material (Figure 3).^[47-49]

2.3. Influencing factors on EMI shielding and microwave absorption characteristics

2.3.1. Dielectric loss

Conductivity loss and polarization loss are the primary causes of dielectric loss.^[50] Polarization loss is further classified as dipole orientation polarization, electronic polarization, ionic polarization, and interfacial polarization.^[51] Based on free electron theory,^[52] $\varepsilon'' = 1/2\pi\rho f \varepsilon_o$, where ρ is the resistivity. A high degree of electrical conductivity, corresponding to a low value of resistivity, raises the value of the imaginary portion of relative complex permittivity. As a result, conductivity loss plays a crucial part in dielectric loss. Ionic and electronic polarization may simply be ignored in EM wave absorption since they

occur at significantly higher frequencies (10^3 – 10^6 GHz).^[53] Dipoles, or bound charges in a dielectric media, are often constrained on the defects and residual groups and, like electrons in an applied electric field, cannot travel freely. Under a high-frequency alternating electric field, the dipoles cannot reorient themselves quickly enough to respond to the external electric field, resulting in dipole orientation polarization and, as a result, relative complex permittivity (ϵ' and ϵ'') begins to decline, resulting in distinct frequency dispersion characteristics. In a heterogeneous system, interfacial polarization and associated relaxation persist at all times, and the accumulation and unequal distribution of space charges at the interfaces provides a macroscopic electric moment that may absorb incoming EM energy well.^[54] The relaxation mechanism can be explained by the Cole-Cole semicircle, which can be construed according to the Debye dipolar relaxation and it can be explained by the following relation between the real part (ϵ') and imaginary part (ϵ'') of complex permittivity^[55]:

$$(\epsilon' - \epsilon_\infty)^2 + (\epsilon'')^2 = (\epsilon_s - \epsilon_\infty)^2$$

where ϵ_s and ϵ_∞ are the static permittivity, and the relative dielectric permittivity at the high-frequency limit, respectively. Under the polarization relaxation mechanism, the curve of ϵ'' and ϵ' will be a single semicircle, known as the Cole-Cole semicircle.

2.3.2. Magnetic loss

Magnetic loss is related to the energy used to transfer magnetic moments in the shielding material, as well as the hysteresis characteristics in response to alternating magnetic field magnetization reversal.^[56] Furthermore, resonances such as domain wall resonance, which normally occurs primarily within the 1 MHz – 100 MHz frequency range, and natural ferromagnetic resonance contribute to the increase of this magnetic loss at certain frequencies. The natural resonance is associated with an anisotropic field and is represented by the natural-resonance formula^[57]:

$$f_r = \gamma H_a / 2\pi$$

where f_r , γ and H_a are the resonance frequency, gyromagnetic ratio, and anisotropy field. The resonance frequency may be modified by varying the anisotropy field of the magnetic nanoparticles, which varies with particle size. The function of eddy current in magnetic loss may be studied by looking at the frequency dependence of μ'' (μ')⁻¹ f^{-1} .^[58] If the value of μ'' (μ')⁻¹ f^{-1} remains constant with frequency variation, eddy current loss is the primary contributor to magnetic loss. Further, eddy current loss, is associated

with the material's magnetic permeability (μ), frequency (f), and conductivity (σ), as follows:

$$C_o = \mu''(\mu')^{-2}f^{-1} = \frac{2}{3} \pi \mu_o d^2 \sigma.$$

2.3.3. Skin depth

At high frequencies, the incoming EM wave only penetrates near the surface of an electrically conductive substance. It is known as the skin effect. The penetration of an electric field of a plane wave into an electrically conductive material decreases exponentially with increasing depth into the electrically conductive shielding material. Skin depth (δ) is the depth at which the field reduces to 1/e, or 37% of the incident value of the field, and it may be calculated using the relation^[59]:

$$\delta = (\pi f \mu \sigma)^{-1}$$

where δ , f , μ are the skin depth, frequency, permeability of the shielding material. The aforementioned relationship indicates that the skin depth (δ) decreases as the frequency and permeability/electrical conductivity of the shielding material rise. The thickness (t), magnetic permeability (μ), and electrical conductivity (σ) of a shield determine its skin depth (δ), which is closely related to SE_A by the relation, $\delta = 1/\sqrt{\pi f \mu} = -8.68(t/SE_A)$.

2.3.4. Impedance matching

The synergistic effects of magnetic and dielectric loss may generate a favorable impedance matching situation and strong EM wave attenuation in the interior of the shielding material, resulting in substantial EM wave absorption.^[60] The modulus of the normalized characteristic impedance $Z = |Z_{in}/Z_o|$ may also be calculated, which represents the ability of the EM wave to penetrate the shielding material and convert to thermal energy.^[61] A value of Z equal to or near to 1 is necessary for high-performance EM wave absorption.

2.3.5. Attenuation constant

After the incident EM waves penetrate the shielding/absorber material, the EM energy is converted to thermal energy by substantial magnetic and dielectric loss. Furthermore, EM wave attenuation in the interior of the shielding/absorber material is crucial due to multiple reflections and scattering in the shielding/absorption material, which may lengthen EM wave propagation routes. The attenuation constant α ^[62] may be used to represent the shielding material's dissipation characteristics:

$$\alpha = \frac{\sqrt{2}\pi f}{c} \sqrt{(\mu''\epsilon'' - \mu'\epsilon') + \sqrt{(\mu''\epsilon'' - \mu'\epsilon')^2 + (\epsilon'\mu'' + \epsilon''\mu')^2}}$$

where f and c are the EM wave propagation frequency and light velocity, respectively. The aforementioned relationship indicates that a higher value of μ'' and ϵ'' of the shielding material might result in a greater value of the attenuation constant.

2.3.6. Another factor

A quarter-wavelength matching model may be used to illustrate the EM wave absorption dependency on shielding material thickness. According to this concept, the following equation^[63] may explain the relationship between shielding material thickness (t_m) and peak frequency (f_m):

$$t_m = nc / (4 f_m (|\epsilon_r| |\mu_r|)^{1/2}); \quad n = 1, 3, 5, \dots$$

where $|\epsilon_r|$ is the modulus of the measured ϵ_r and $|\mu_r|$ is the modulus of the measured μ_r at the peak frequency (f_m). If the computed t_m agrees with the observed matching thickness t_m , the EM wave absorption adheres to the quarter-wavelength matching model.

3. Carbon nanotube and spinel ferrite based nanocomposites

3.1. Carbon nanotube and Fe₃O₄ based nanocomposites

In recent years, Fe₃O₄ has received a lot of attention among spinel ferrite magnetic loss materials because of its effective electromagnetic wave absorption properties, cheap manufacturing cost, and good environmental friendliness. Furthermore, numerous carbon nanotubes based on Fe₃O₄ magnetic nanocomposites with excellent impedance matching and strong EM wave absorption capacities have been reported (Table 1). Lingyu Zhu *et al.*,^[64] for example, demonstrated a programmable modification of complicated permittivity by connecting uniform Fe₃O₄ magnetic porous spheres onto carbon nanotubes (CNTs) to build a 3D network. Fe₃O₄/CNTs nanocomposites were created using a simple one-pot solvothermal technique that was both time and energy efficient. To explore the effect of CNT content on EM wave absorption properties, four samples were developed:

Fe₃O₄, Fe₃O₄/3 wt% CNTs, Fe₃O₄/5 wt% CNTs, and Fe₃O₄/7 wt% CNTs, each comprising 0, 3, 5, and 7 wt% CNTs. The produced nanocomposite (50 wt%) and paraffin wax (50 wt%) were evenly mixed and compacted into toroidal forms with 3 mm internal diameter and 7 mm outer diameter for EM wave absorption measurements in the frequency range 2–18 GHz. The thickness of the generated sample was used to study reflection loss (RL) and effective bandwidth (RL –10 dB), which are important factors for assessing the application possibilities of EM wave absorption materials. Fe₃O₄/5 wt% CNTs composites demonstrated excellent EM wave absorption, with a minimum RL value of –51.32 dB at 5.52 GHz and 4.4 mm sample thickness (Figure 4). Fe₃O₄/5 wt% CNTs composites had an effective bandwidth of 3.9 GHz. It was attributable to the produced Fe₃O₄/5 wt% CNTs composites material's superior polarization relaxation and high dielectric loss. Furthermore, when the sample thickness of Fe₃O₄/CNTs composites increased, the absorption peak became sharper and the matching frequency (f_m) migrated to a lower frequency. These observed phenomena were in accordance with the quarter-wavelength cancelation rule.^[65]

To further understand the EM process for EM wave absorption, the impedance matching of produced nanocomposites was examined. The value of Z (Z_{in}/Z_0) for Fe₃O₄/5 wt% CNTs composite was almost equal to 1, indicating that the materials had excellent impedance matching (Figure 5a). The excellent impedance matching level was linked to synergistic interactions between Fe₃O₄ magnetic spheres and high-conductivity CNTs. Because of the substantial dielectric loss as well as interfacial polarization, electron hopping (Figure 5d), and magnetic loss from magnetic Fe₃O₄ porous spheres, the produced Fe₃O₄/CNTs composites EM wave absorber (Figure 5b) can attenuate practically all EM waves (Figure 5c). This study group developed a simple way for improving the EM wave absorption properties of Fe₃O₄/CNTs composites and encouraged its future use in the area of efficient EM wave absorber materials.

In addition, Xiaojun Zeng *et al.*^[66] studied the EMI shielding properties of a three-dimensional (3-D)

Table 1. Summary of recent progress on carbon nanotube and Fe₃O₄ based nanocomposites.

No.	Shielding material	Frequency band	Optimum thickness	Effect of shielding	Ref.
1.	Fe ₃ O ₄ /5 wt% CNTs	2–18 GHz	4.4 mm	–51.32 dB	[52]
2.	Fe ₃ O ₄ /CNTs	2–18 GHz	2.15 mm	–56.8 dB	[54]
3.	Fe ₃ O ₄ /MWCNTs	2–18 GHz	4 mm and 2 mm	–36 dB	[67]
4.	Fe ₃ O ₄ / MWCNTs	2–18 GHz	6.8 mm	–52.8 dB	[68]
5.	Fe ₃ O ₄ / MWCNTs	2–18 GHz	3.4 mm	–41.61 dB	[69]
6.	SiO ₂ @Fe ₃ O ₄ /MWCNT	8–12 GHz	4 mm	–41dB	[70]

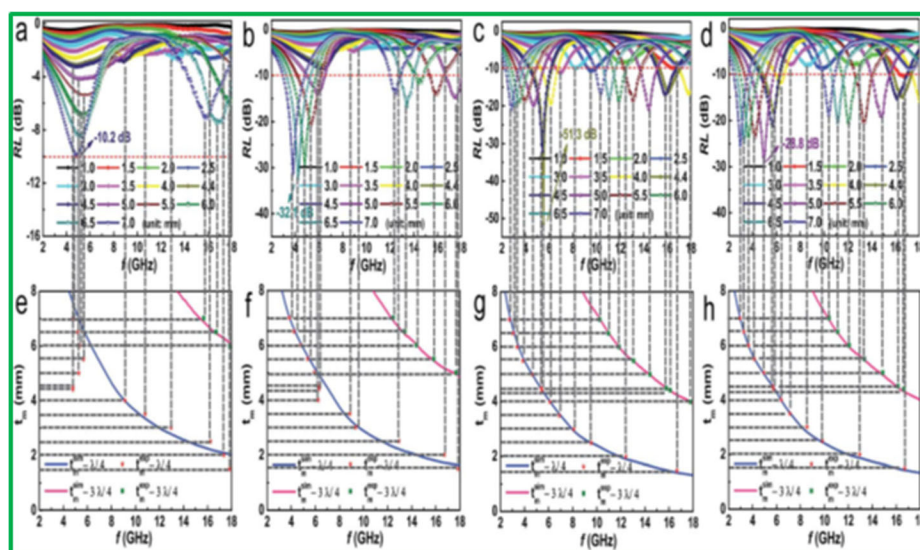


Figure 4. RL curves of Fe₃O₄ sample (a), Fe₃O₄/3 wt% CNTs (b), Fe₃O₄/5 wt% CNTs (c), and Fe₃O₄/7 wt% CNTs (d) composites. The dependence of t_m on f_m for Fe₃O₄ sample (e) and Fe₃O₄/CNTs composites (f–h) at wavelengths of $1/4$ and $3/4$. Reproduced with permission from Ref. [64]. Copyright 2017. RSC Publication.

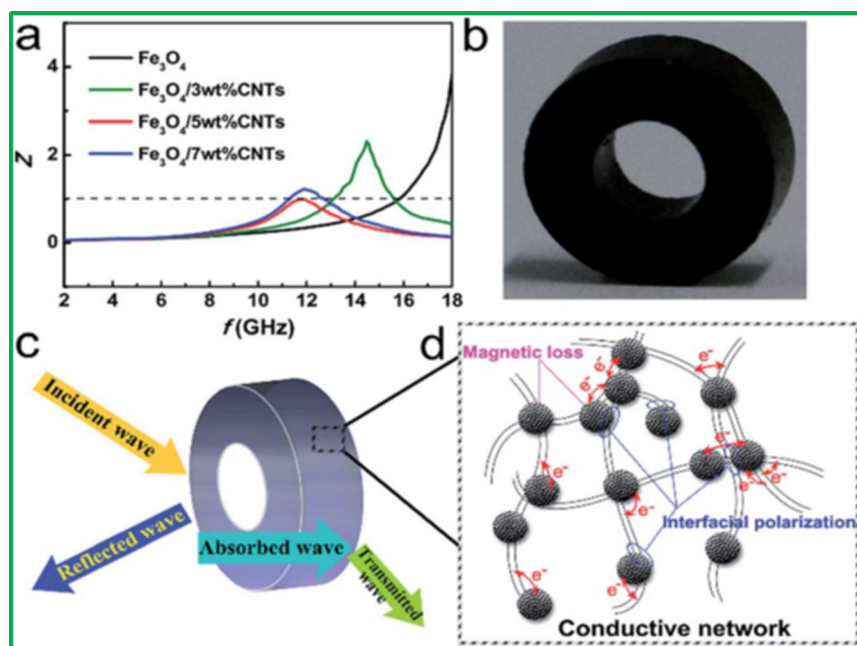


Figure 5. (a) The frequency-dependent Z values of Fe₃O₄ sample and Fe₃O₄/CNTs composites. (b) Image of the real product for the absorber. (c, d) Scheme of primary EM microwave attenuation processes involved in Fe₃O₄/CNTs composites absorber. Reproduced with permission from Ref. [64]. Copyright 2017. RSC Publication.

hierarchical urchin-like Fe₃O₄/CNTs design. A simple hydrothermal approach was used to create the 3-D hierarchical urchin-like Fe₃O₄/CNTs constructions. Fe₃O₄/3CNTs, Fe₃O₄/5CNTs, and Fe₃O₄/7CNTs were the names given to composites made with 0 wt%, 3 wt%, 5 wt%, and 7 wt% CNTs. CNTs serve as conductive skeletons in the proposed system, forming enormous contacts with Fe₃O₄. The addition of CNTs significantly improved the dielectric properties and impedance matching level of the constructed design.

As shown in Figure 6, the developed Fe₃O₄/CNTs design had a reflection loss (RL) of -56.8 dB at 11.12 GHz and a thin thickness of 2.15 mm. Furthermore, the synergistic influence of conduction loss, interfacial polarization, natural resonance, eddy current loss, and multiple reflection/scattering was connected with the high EM wave absorption properties of hierarchical Fe₃O₄/CNTs design. Using magnetic Fe₃O₄ and carbon nanotubes, this study developed a robust technique for 3-D hierarchical

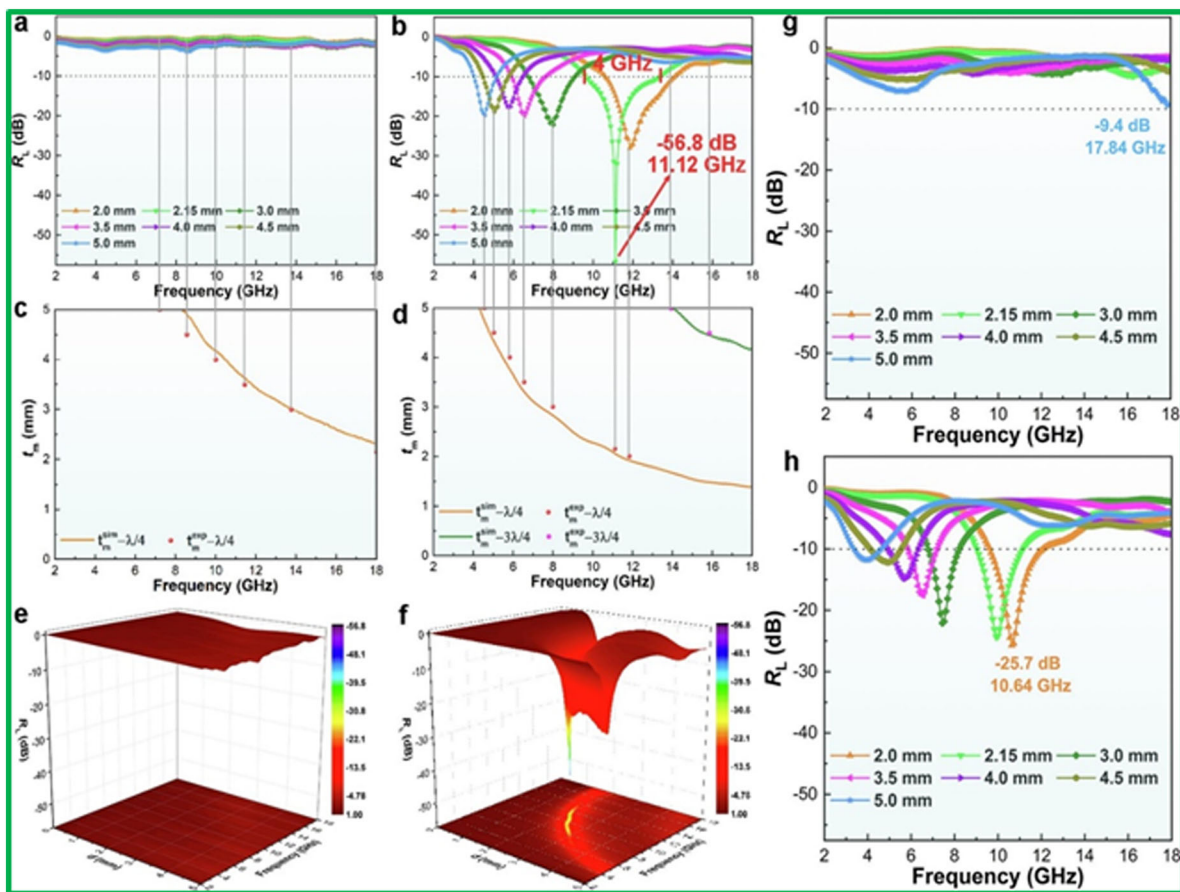


Figure 6. The 2-D RL (a, b) and 3-D RL (e, f) curves for Fe_3O_4 (a, e) and $\text{Fe}_3\text{O}_4/5\text{CNTs}$ (b, f). Corresponding t_m dependences of f_m at wavelengths of $\lambda/4$ and $3\lambda/4$ (c, d). 2-D RL curves for $\text{Fe}_3\text{O}_4/3\text{CNTs}$ (g) and $\text{Fe}_3\text{O}_4/7\text{CNTs}$ (h). Reproduced with permission from Ref. [66]. Copyright 2022. Elsevier Publication.

structure building for high-performance EM wave absorption. It was also noticed that the relationship between matching thickness (t_m) and matching frequency (f_m) of $\text{Fe}_3\text{O}_4/5\text{CNTs}$ matched well with the quarter-wavelength matching conditions (Figure 6).

$\text{Fe}_3\text{O}_4/\text{MWCNTs}$ nanocomposites were described by Honglei Yuan et al.^[67] as having noticeably improved EM wave absorption properties in the high frequency (Ku-band) range. For nanocomposites with thicknesses of 1.5 - 5 mm and a frequency range of 2–18 GHz, it was observed that all minimal RL values were less than -20 dB; however, at 5 GHz and 12.6 GHz, where the thickness was 4 mm and 2 mm, respectively, the minimal RL was reduced to -36 dB. The detailed contour map of reflection loss values versus frequency at various thicknesses for $\text{Fe}_3\text{O}_4/\text{MWCNTs}$ hybrids (Figure 7) shows two strong RL sections at high frequency and low frequency ranges, respectively. Additionally, it was clear that the simulations (Figure 7b) using the $1/4$ condition for $\text{Fe}_3\text{O}_4/\text{MWCNTs}$ hybrid were in good agreement with the relationship between the experimental matching thickness and peak frequency (Figure 7a). The

observed results showed that the quarter-wave theory can adequately explain the relationship between matching thickness and frequency for the EM wave absorption.

Yi-Hua Chen et al.^[68] reported 3D Fe_3O_4 nanocrystals decorating carbon nanotubes to modify electromagnetic properties and improve microwave absorption capacity. In the frequency range of 2–18 GHz, the minimum reflection loss values at 20 wt% loading and a thickness of 6.8 mm of -23.0 dB and -52.8 dB were observed at 4.1 GHz and 12.8 GHz, respectively, which were superior to those of pure MWCNTs as well as other hybrids of Fe_3O_4 . The improved absorption capacity arises from the synergy of dielectric loss and magnetic loss, as well as the enhancement of multiple interfaces among 3D Fe_3O_4 nanocrystals. Zhijiang Wang et al.^[69] reported a hybrid material consisting of magnetite (Fe_3O_4) nanocrystals grown on multiwalled carbon nanotube (MWCNT) as a high-performance microwave absorber in the 2–18 GHz band. The hybrid material exhibited considerable electromagnetic absorbing ability, with minimum reflection loss reaching -41.61 dB

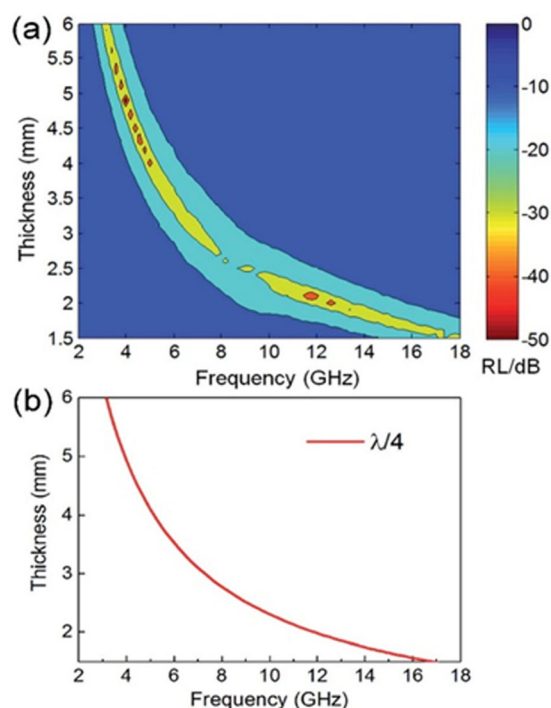


Figure 7. (a) Color map of the RL values calculated from the measured electromagnetic parameters, and (b) dependence of $\lambda/4$ thickness on frequency for the nanocomposite. Reproduced with permission from Ref. [67]. Copyright 2016. RSC Publication.

at a frequency of 5.5 GHz and thickness of 3.4 mm. Hoda Hekmatara et al.^[70] investigated the microwave absorption properties of core-shell composites containing; iron oxide decorated carbon nanotubes (CNT) and silica ($\text{SiO}_2@Fe_3O_4/\text{MWCNT}$) with various thickness of silica shell (7, 20 and 50 nm). It was noticed that the minimum reflection loss decreased with increasing SiO_2 thickness. The minimum reflection loss of the composite with an optimized thickness of silica shell (7 nm) exceeded -41dB at 8.7–9 GHz.

3.2. Carbon nanotube and CoFe_2O_4 based nanocomposites

Cobalt ferrite (CoFe_2O_4) has been extensively explored as an EM wave absorber material among the spinel ferrites. CoFe_2O_4 has moderate saturation magnetization, strong anisotropy, high resistivity, high hysteresis loss, excellent chemical stability, high oxidation resistance, good corrosion resistance, and cheap manufacturing costs.^[71] Furthermore, because to its high density, narrow absorption bandwidth, and poor impedance matching, its technical uses are limited.^[72] Furthermore, owing to their low density, strong

Table 2. Summary of recent progress on carbon nanotube and CoFe_2O_4 based nanocomposites.

No.	Shielding material	Frequency band	Optimum thickness	Effect of shielding	Ref.
1.	$\text{CoFe}_2\text{O}_4/\text{MWCNTs}$	2–18 GHz	4.2 mm	-50.80 dB	[58]
2.	$\text{CoFe}_2\text{O}_4/\text{MWCNTs}$	2–18 GHz	1.5 mm	-46.65 dB	[60]
3.	$\text{CoFe}_2\text{O}_4/\text{CNTs}$	2–18 GHz	1.7 mm	-37.39 dB	[61]
4.	$\text{CoFe}_2\text{O}_4/\text{MWCNTs}$	2–18 GHz	1.9 mm	-36.52 dB	[78]

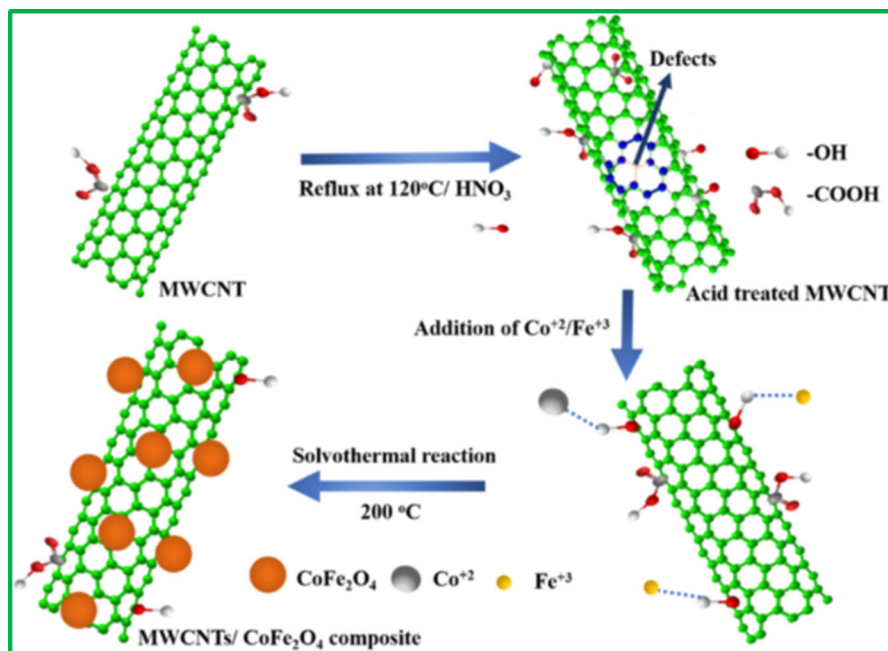


Figure 8. Schematic diagram explaining synthesis of $\text{CoFe}_2\text{O}_4/\text{MWCNTs}$ composites. Reproduced with permission from Ref. [74]. Copyright 2022. Elsevier Publication.

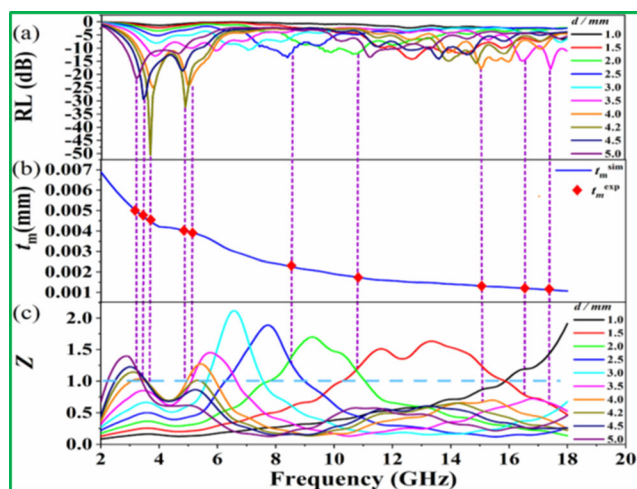


Figure 9. (a) Frequency-dependence RL with different thicknesses, (b) simulations of the t_m versus f_m under the $1/4 \lambda$ model, and (c) impedance matching (Z) as a function of frequency with different thicknesses for S2 composite. Reproduced with permission from Ref. [74]. Copyright 2022. Elsevier Publication.

chemical stability, and high conduction loss, multi-walled carbon nanotubes (MWCNTs) have been identified as EM wave absorbers. As a result, MWCNTs with high conductivity, surface area, and light weight were added to CoFe_2O_4 magnetic spinel ferrite to create nanocomposites with excellent EM wave absorption capabilities (Table 2).^[73]

M. Zeeshan Ashfaq et al.^[74] recently disclosed a cobalt ferrite/MWCNTs ($\text{CoFe}_2\text{O}_4/\text{MWCNTs}$) hybrid composite for expanded bandwidth EM wave absorption. This study group used a simple and controlled solvothermal process (Figure 8) to create $\text{CoFe}_2\text{O}_4/\text{MWCNTs}$ composites and then investigated the influence of MWCNTs content 0 mg, 10 mg, and 20 mg on microwave absorption properties for samples indicated as S1, S2, and S3, respectively. The wax, which is transparent to electromagnetic waves, was mixed homogeneously with composites in a weight percentage of 50% and then pressed into a toroidal ring-shaped sample 2.0 mm in diameter for electromagnetic parameter measurements. The S2 composite has an RL_{\min} of -50.80 dB at 4.2 mm thickness and an effective absorption bandwidth (EAB) of 3.36 GHz at 1.6 mm thickness. The quarter-wavelength matching theory^[75] was used to study the connection between absorption peak frequency (f_m) and coating thickness (t_m) for S2 composite, as illustrated in Figure 9(a) and 9(b). The RL peaks in the S2 composite sample moved to lower frequencies as the t_m increased (Figure 9a). Furthermore, it had the best RL peak (3.68 GHz at 4.2 mm) at the ideal impedance ($Z \approx 1$), (Figure 9c). Conduction loss due to free electrons hopping inside

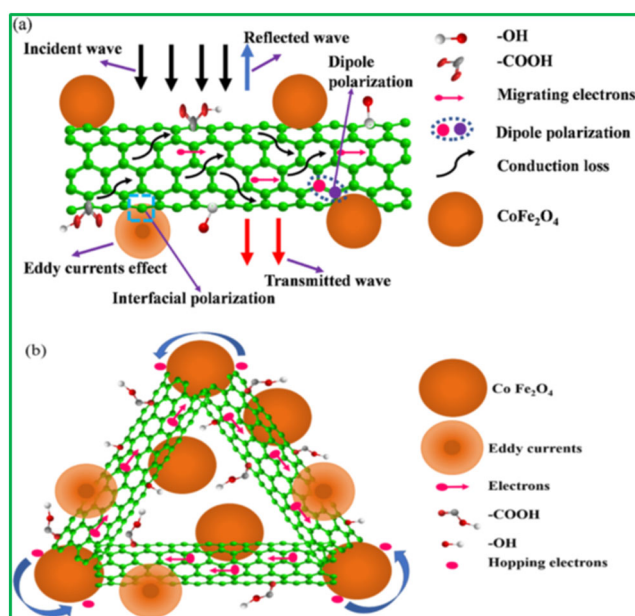


Figure 10. Schematic illustration of the possible microwave absorption mechanisms of $\text{CoFe}_2\text{O}_4/\text{MWCNT}$ composites. Reproduced with permission from Ref. [74]. Copyright 2022. Elsevier Publication.

the conducting network of the MWCNTs, dielectric loss, magnetic loss, electromagnetic attenuation, impedance matching, dipole, interfacial, and defect polarization were all connected with EM wave absorption (Figure 10).

Furthermore, Hongmei Liu et al.^[76] discovered that cobalt ferrite microspheres/multi-walled carbon nanotube composites had high-performance EM wave absorption properties. A simple one-step solvothermal process was used to create CoFe_2O_4 and MWCNTs composites. The produced composites were evenly mixed with paraffin (50 wt%) and pressed into a cylindrical toroid shape with 3.04 mm inner diameter and 7.00 mm outside diameter for EM parameter measurements. The dielectric constant was found to rise dramatically as the loadings of MWCNTs in the composites increased. At 14.4 GHz, the RL_{\min} of a composite containing 3 wt% CNTs was -46.65 dB, with an effective absorption bandwidth of 4.91 GHz (12.41 to 17.32 GHz) at a thin thickness of 1.5 mm. Yue Yuan et al.^[77] also explored the effect of CNTs on the EM wave absorption properties of CoFe_2O_4 nanoparticles. A simple solvothermal technique was used to create $\text{CoFe}_2\text{O}_4/\text{CNTs}$ nanocomposite materials. At a thickness of 1.7 mm, the reflection loss of $\text{CoFe}_2\text{O}_4/\text{CNTs}$ was -37.39 dB, and the effective absorption bandwidth was 5.2 GHz. In compared to pure cobalt ferrite, the produced composite demonstrated superior microwave absorption. Danqiang Huang et al.^[78] reported MWCNTs wrapped in

Table 3. Summary of recent progress on carbon nanotube and NiFe₂O₄ based nanocomposites.

No.	Shielding material	Frequency band	Optimum thickness (mm)	Effect of shielding	Ref.
1.	NiFe ₂ O ₄ /MWCNTs	2–18 GHz	1.5 mm	–19 dB	[80]

Table 4. Summary of recent progress on carbon nanotube and mixed spinel ferrite based nanocomposites.

No.	Shielding material	Frequency band	Optimum thickness	Effect of shielding	Ref.
1.	Mg-Ni spinel ferrite-MWCNT /Cu	8–18 GHz	1.5 mm	–39.72 dB	[82]
2.	MWCNTs/Ni _{0.5} Zn _{0.5} Nd _{0.04} Fe _{1.96} O ₄	2–18 GHz	1.6 mm	–35.05 dB	[83]
3.	MWCNTs/Ni _{0.5} Zn _{0.5} Fe ₂ O ₄	8–12 GHz	3 mm	–19.34 dB	[84]
4.	Ni _{0.3} Zn _{0.4} Co _{0.2} Cu _{0.1} Fe ₂ O ₄ / MWCNTs	8–18 GHz	1 mm	–25.71 dB	[85]
5.	Li _{0.3} Zn _{0.4} Fe _{2.3} O ₄ @CNT	0.2–20 GHz	5 mm	–34 dB	[87]

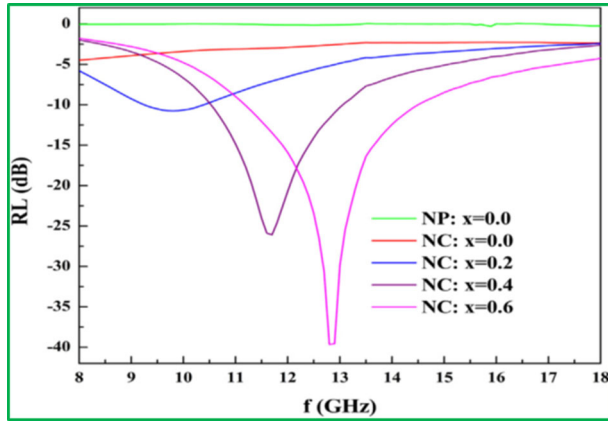


Figure 11. The reflection loss of the Mg_{0.6}Ni_{0.4}Fe₂O₄ nanoparticles (NP: $x = 0.0$) and Mg_{0.6-x}Ni_{0.4}Cu_xFe₂O₄-MWCNT nanocomposites (NC: $x = 0.0, 0.2, 0.4$ and 0.6). Reproduced with permission from Ref. [82]. Copyright 2019. Elsevier Publication.

hollow with open holes of CoFe₂O₄ as an outstanding electromagnetic wave absorber. Multiwalled carbon nanotubes (MWCNTs) induce dipole polarization when incorporated, and when wrapped around CoFe₂O₄ particles, this increases interface loss. The maximum electromagnetic wave absorption characteristic was attained at 25% filling with a RL_{min} of –36.52 dB at a thickness of 1.9 mm and an effective absorption bandwidth (EAB) of 3 GHz.

3.3. Carbon nanotube and NiFe₂O₄ based nanocomposites

Nickel ferrite (NiFe₂O₄) is a good dielectric material as well as an EM wave absorber in the spinel ferrite family.^[79] The EM wave absorption properties of NiFe₂O₄ spinel ferrite may be enhanced further by increasing dielectric loss by including MWCNTs with the ferrite. Lei Guo et al.^[80] used the hydrothermal technique to describe microwave absorption properties of NiFe₂O₄/MWCNTs hybrids. At 11.3 GHz, the optimized sample had a RL_{min} of –19 dB and a bandwidth of 2.5 GHz at a thickness of 1.5 mm (Table 3).

3.4. Carbon nanotube and mixed spinel ferrite based nanocomposites

Doping/substitution of various elements in spinel ferrite might result in an effective augmentation of magnetic properties as well as an improvement in EM wave absorption.^[81] Because of its superior EM wave absorption qualities, mixed spinel ferrite with MWCNTs has been intensively explored in EM wave absorption materials in recent years (Table 4). M. Rostami et al.^[82] examined the EM wave absorption properties of Mg-Ni spinel ferrite-MWCNT nanocomposites with Cu substitution. It was discovered that replacing Cu with MWCNTs may considerably improve the EM wave absorption of nanocomposites (Figure 11). At a thickness of just 1.5 mm, the greatest reflection loss was –39.72 dB, which was related with proper impedance matching and the coexistence of both dielectric and magnetic loss.

Ningyu Chen et al.^[83] also looked into the EM wave absorption properties of Nd-doped Ni-Zn ferrite/multi-walled carbon nanotubes (MWCNTs) composites. The MWCNTs/Ni_{0.5}Zn_{0.5}Nd_{0.04}Fe_{1.96}O₄ composites were created using the sol-gel method and sintered at high temperatures with argon gas. S0 signified pure Ni_{0.5}Zn_{0.5}Nd_{0.04}Fe_{1.96}O₄ (NZNF), whereas S1, S2, and S3 denoted composites containing 1 wt%, 1.5 wt%, and 2 wt% MWCNTs, respectively. The S2 sample has an RL_{min} of –35.05 dB at 1.6 mm thickness and an effective absorption bandwidth of 4.55 GHz (Figure 12). The reflection loss curves of the samples at various thicknesses showed that the RL_{min} that moves to the lower frequency with the thickness increases. The $\lambda/4$ matching theory can be used to shed light on the connection between thickness and frequency. It was observed that the RL_{min} of S2 moves to low frequency when the thickness increases (Figure 13). Particularly when all matching thickness (t_m) were close to the $\lambda/4$ curves, as Z_{in} at 1.6 mm was close to 1, indicated that the material with such thickness had the outstanding absorption performance. Overall, there was high consistency in the RL_{min},

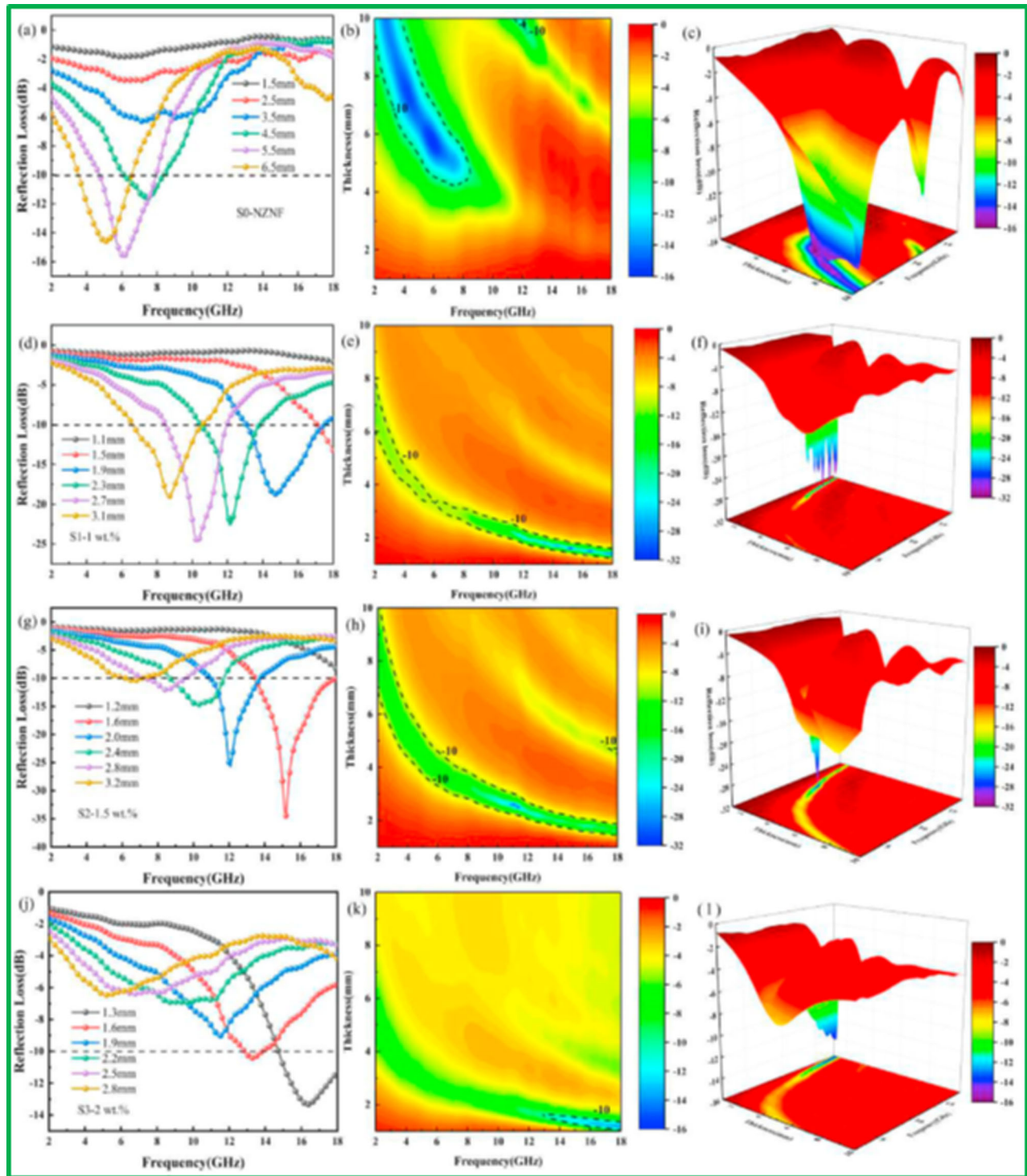


Figure 12. Reflection loss with a series of thickness, contour maps of reflection loss, and three-dimensional reflection loss for (a–c) S0, (d–f) S1, (g–i) S2, (j–l) S3. Reproduced with permission from Ref. [83]. Copyright 2021. Elsevier Publication.

quarter-wavelength, and impedance matching relationships of S2.

M. S. Mustafa et al.^[84] went on to examine the EM wave absorption properties of multiwalled carbon nanotubes/ $\text{Ni}_{0.5}\text{Zn}_{0.5}\text{Fe}_2\text{O}_4$. At a thickness of 3 mm, the produced composite had a maximum reflection loss (RL) of -19.34 dB at 8.46 GHz and a bandwidth

of 1.24 GHz. M. Dalal et al.^[85] also looked into the microwave absorption capabilities of $\text{Ni}_{0.3}\text{Zn}_{0.4}\text{Co}_{0.2}\text{Cu}_{0.1}\text{Fe}_2\text{O}_4$ nanoparticles enclosed in multiwalled carbon nanotubes. The greatest value of reflection loss was -25.71 dB at 15.24 GHz for an enclosed composite sample with a layer thickness of 1 mm. M. Chahar et al.^[86] have looked into the microwave

absorption characteristics of MWCNT/zinc-doped nickel ferrite nanocomposites. Co-precipitation and physical mixing were used to create MWCNTs and $\text{Ni}_{0.5}\text{Zn}_{0.5}\text{Fe}_2\text{O}_4$ -based nanocomposites. The greatest reflection loss (RL) for a nanocomposite synthesized using the physical-mixing technique was -51.2 dB at 11.2 GHz with a bandwidth of 0.45 GHz. Furthermore, Yu Gao et al.^[87] examined the microwave absorption characteristics of a combination of Li-Zn ferrite and carbon nanotubes. A simple mechanical mixing approach was used to create a nanocomposite made of carbon nanotubes and $\text{Li}_{0.3}\text{Zn}_{0.4}\text{Fe}_{2.3}\text{O}_4$ nanoparticles (LiZn@CNT). At a thickness of 5 mm, the lowest reflection loss (RL) was -34 dB and the absorption bandwidth was 5.2 GHz.

4. Graphene, carbon nanotube, and spinel ferrite based nanocomposites

In recent years, graphene has been used with spinel ferrite and carbon nanotube composite systems to

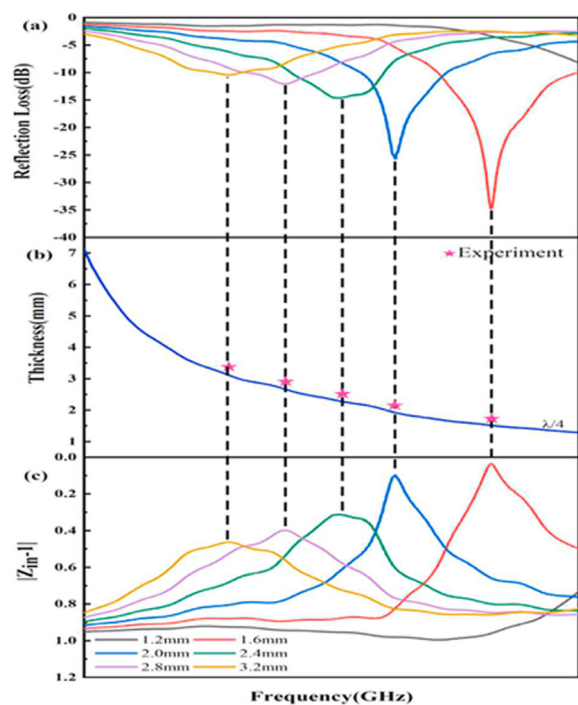


Figure 13. (a) Reflection loss curve, (b) matching of thickness under the $\lambda/4$ models, and (c) $|Z_{in} - 1|$ of different thickness for S2 with different thicknesses. Reproduced with permission from Ref. [83]. Copyright 2021. Elsevier Publication.

increase microwave absorption (Table 5). The ternary composite system demonstrated superior microwave absorption features such as low reflection loss and absorption bandwidth. Y. Zhou et al.,^[88] for example, reported the microwave absorption characteristics of RGO/MWCNT/ Fe_3O_4 hybrids (GMFs) manufactured using an *in situ* one-pot solvothermal approach (Figure 14). GMF0, GMF1, GMF3, GMF5, GMF7, and GMF15 samples were indicated as GMF0, GMF1, GMF3, GMF5, GMF7, and GMF15, respectively, based on raw material ratios of 0.00, 0.01, 0.03, 0.05, 0.07, and 0.15 g of GO.^[88] Toroidal samples with inner diameters of 3.04 mm, exterior diameters of 7.00 mm, and sample thicknesses of 2.00–3.50 mm were created by homogeneously combining paraffin wax with hybrids (mass ratio = 4:6). GMF5 hybrid produced at a solvothermal reaction time of 24 h with a mass ratio of 5:1:73 of GO, MWCNT, and Fe_3O_4 displayed a maximum RL value of -61.29 dB at 10.48 GHz at a thickness of just 2.6 mm (Figure 15).

For GMF5, the numerous Fe_3O_4 cluster crystal interfaces, the numerous combined Fe_3O_4 , RGO, and MWCNT interfaces, the porous GMF structure, and the suitable RGO and MWCNT contents regulate the electromagnetic parameters, which were advantageous for wave attenuation, energy conversion, and fitting to an excellent MA property.

Furthermore, R. Shu et al.^[89] examined the microwave absorption properties of a hybrid composite of reduced graphene oxide/multi-walled carbon nanotubes/zinc ferrite (RGO/MWCNTs/ ZnFe_2O_4). A simple

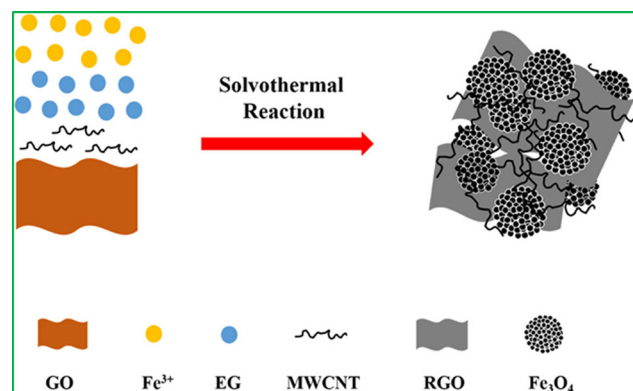


Figure 14. Schematic of the Synthesis Procedure of the GMFs. Reproduced with permission from Ref. [88]. Copyright 2020. ACS Publication.

Table 5. Summary of recent progress on graphene, carbon nanotube, and spinel ferrite based nanocomposites.

No.	Shielding material	Frequency band	Optimum thickness	Effect of shielding	Ref.
1.	RGO/MWCNT/ Fe_3O_4	2–18 GHz	2.6 mm	-61.29 dB	[88]
2.	RGO/MWCNTs/ ZnFe_2O_4	2–18 GHz	1.0 mm	-22.2 dB	[89]
3.	Fe_3O_4 @MWCNTs/RGO	8.2–12.4 GHz	0.6 mm	45.9 dB	[90]

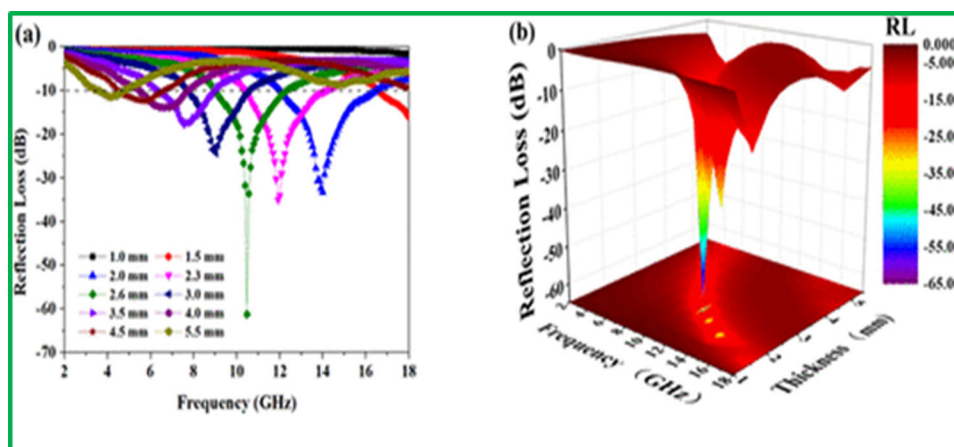


Figure 15. (a, b) Frequency-dependent RL curves and 3D maps of GMF5. Reproduced with permission from Ref. [88]. Copyright 2020. ACS Publication.

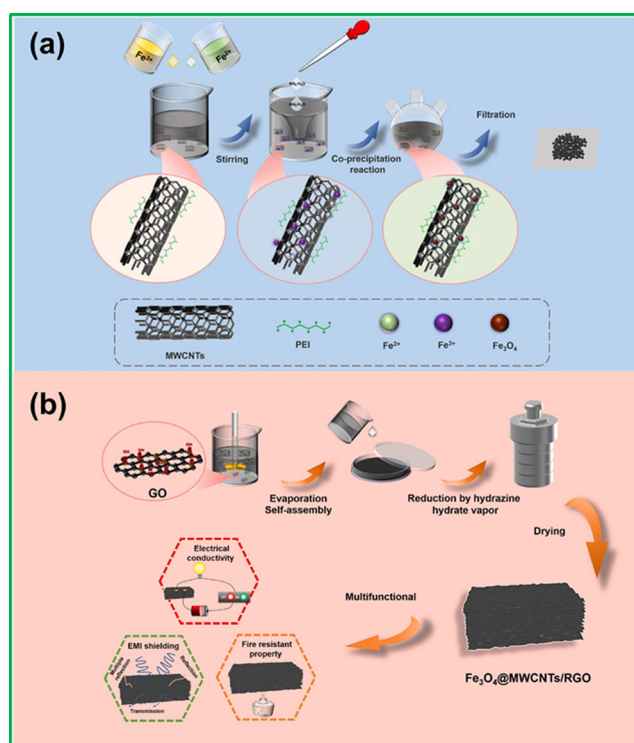


Figure 16. Illustrations for the preparation of (a) $\text{Fe}_3\text{O}_4@\text{MWCNTs}$ and (b) $\text{Fe}_3\text{O}_4@\text{MWCNTs}/\text{RGO}$. Reproduced with permission from Ref. [90]. Copyright 2022. Elsevier Publication.

solvothermal approach was used to create the ternary composite. By twisting MWCNTs around ZnFe_2O_4 microspheres and interconnecting them with RGO, a highly connected three-dimensional conductive network was created in the ternary composite. At a thickness of just 1.0 mm, the created ternary composite system had a minimum reflection loss of -22.2 dB and a maximum absorption bandwidth of 2.3 GHz. The microwave absorption mechanism of such a composite was related with enhanced conductivity loss, a

synergistic impact of magnetic and dielectric loss, moderate impedance matching, and significant attenuation loss.

Juanjuan Zhou et al.^[90] have explored the EMI shielding properties of an advanced ternary nanocomposite paper system comprising graphene and Fe_3O_4 with multi-walled carbon nanotubes (MWCNTs). As shown in Figure 16, advanced $\text{Fe}_3\text{O}_4@\text{MWCNTs}/\text{RGO}$ nanocomposite paper was created *via* evaporation-assisted self-assembly and hydrazine hydrate vapor reduction. It was discovered that the filling amount of $\text{Fe}_3\text{O}_4@\text{MWCNTs}$ and the thickness of the paper may be used to modify the EMI shielding efficiency (SE). The total SE of the composite paper in the X-band was 45.9 dB, with a thickness of about 0.6 mm and a mass percentage of $\text{Fe}_3\text{O}_4@\text{MWCNTs}$ of 2%; it was also 31.14% greater than the pure RGO paper (~ 35 dB) (Figure 17). $\text{Fe}_3\text{O}_4@\text{MWCNTs}/\text{RGO}$ composite papers' increased SE_{total} was primarily due to increased absorption rather than reflection. According to the proportion of EM wave transmission (T), absorption (A), and reflection (R); the absorption efficiency-rather than reflection efficiency-plays a major role in the SE of composite papers (supplementary material^[90]). It was also observed that the average SE_{total} of $\text{Fe}_3\text{O}_4@\text{MWCNTs}/\text{RGO}$ changed with the thickness of the paper (Figure 17). Because of the impedance mismatch between the composites and air, some of the incident EM waves were reflected on the surface of the developed paper; nevertheless, the remainder of the incident EM waves entered the produced paper. The Fe_3O_4 particle-induced conduction channel in the $\text{Fe}_3\text{O}_4@\text{MWCNTs}$ heterostructure may promote the connection of MWCNTs in the composite to build a conductive network, and it can be cooperative to consume the EM wave within this

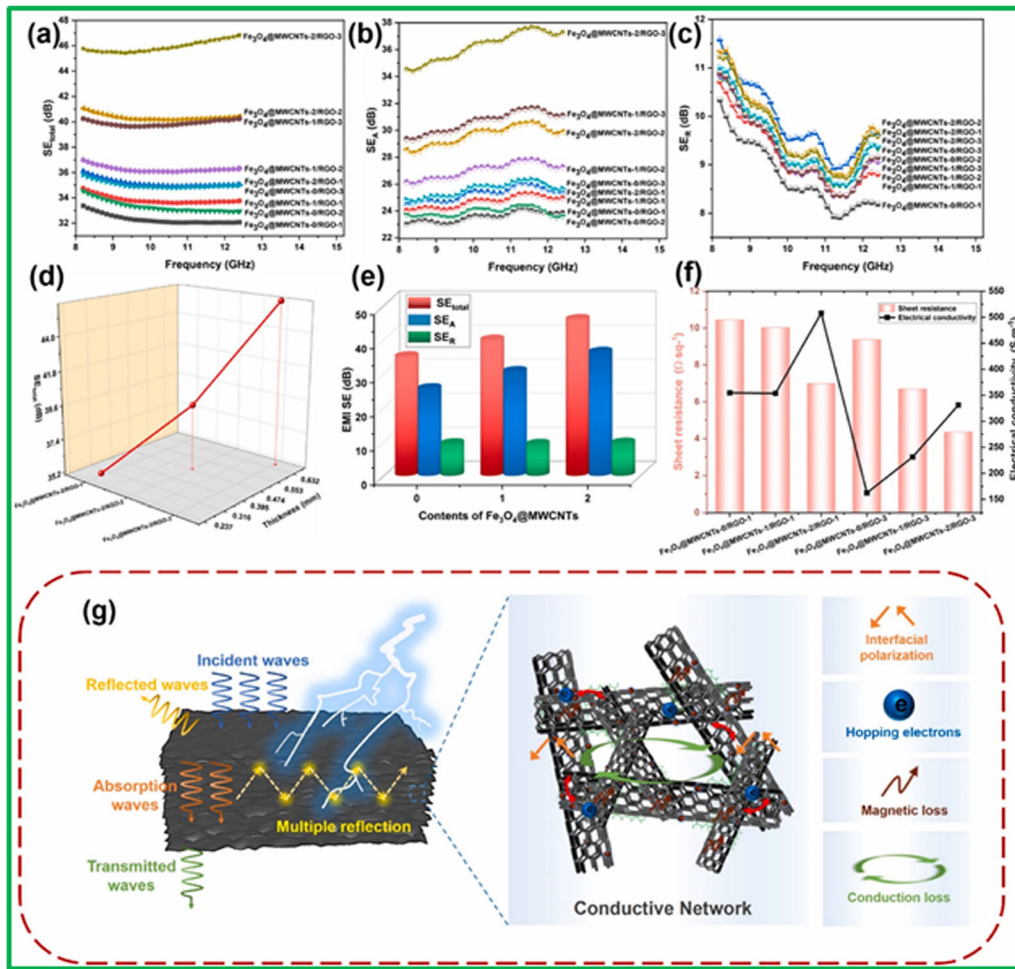


Figure 17. EMI shielding property of different composite papers: (a) SE_{total} , (b) SE_A , and (c) SE_R values; (d) SE_{total} values with different paper's thicknesses; (e) EMI SE values of composite papers with diverse $Fe_3O_4@MWCNTs$ loadings; (f) sheet resistance and electrical conductivity of composite papers; (g) schematic diagram of EMI shielding mechanism. Reproduced with permission from Ref. [90]. Copyright 2022. Elsevier Publication.

Table 6. Summary of recent progress on carbon, carbon nanotube, and spinel ferrite based nanocomposites.

No.	Shielding material	Frequency band	Specimen thickness	Effect of shielding	Ref.
1.	$Fe_3O_4 / MWCNTs@C$	2–18 GHz	2.0 mm	−52.47 dB	[91]
2.	$(Zn_{0.5}Co_{0.5}Fe_2O_4/Mn_{0.5}Ni_{0.5}Fe_2O_4)@C-MWCNTs$	0–3 GHz	5 mm	−35.14 dB	[92]

composite paper. Additionally, the presence of Fe_3O_4 nanoparticles might increase dielectric and magnetic losses. The attenuation of electromagnetic waves caused by repeated internal reflections in cavities formed between composite paper layered structures cannot be overlooked.

5. Carbon, carbon nanotube, and spinel ferrite based nanocomposites

Carbon has recently been combined with carbon nanotubes and spinel ferrite to improve EM wave absorption qualities (Table 6). K. Zhang et al.,^[91] for example, studied the EM wave absorption properties of Fe_3O_4 nanoparticles with MWCNTs@C ferrite

nanocomposites. These nanocomposites were created using a co-precipitation and calcination approach. Fe_3O_4 nanoparticles with MWCNTs@C ferrite nanocomposites with Fe_3O_4 nanoparticle contents of about 50%, 60%, and 68% were created and designated as samples-1, sample-2, and sample-3, respectively. Toroid form samples were generated for microwave characteristics assessment by combining 20% of the prepared composite with 80% paraffin wax. The Fe_3O_4 nanoparticles with MWCNTs@C ferrite composite systems with roughly 60% Fe_3O_4 nanoparticles had a maximum reflection loss of −52.47 dB at 10.4 GHz and a bandwidth of 3.6 GHz at a thickness of 2.0 mm (Figure 18). The magnetic spinel ferrite nanoparticle composition has an effect on the EM

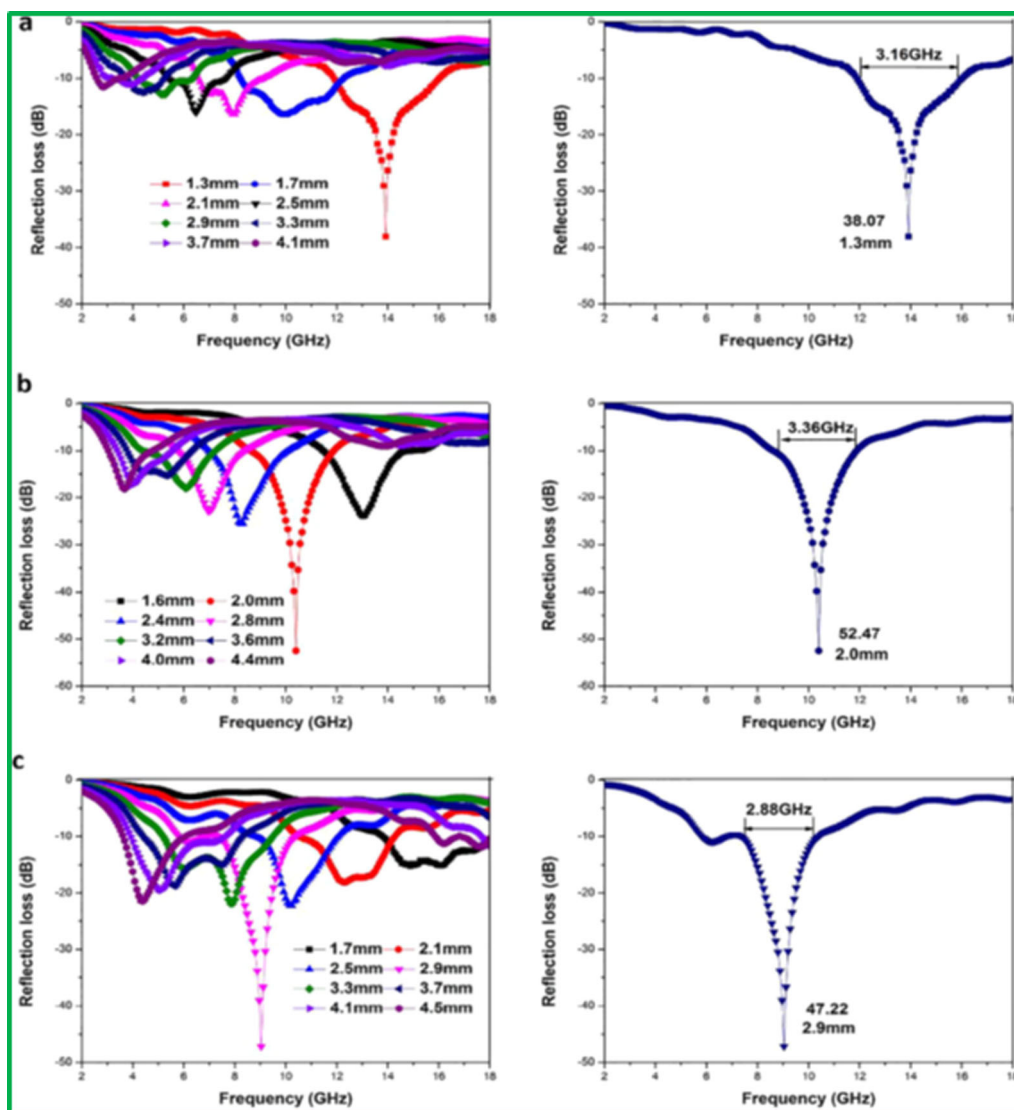


Figure 18. Reflection loss curves and the corresponding bandwidth of the maximum reflection loss that was below -10 dB of the prepared composites: sample-1 (a); sample-2 (b) and sample-3 (c). Reproduced with permission from Ref. [91]. Copyright 2018. Elsevier Publication.

Table 7. Summary of recent progress on MXene, carbon nanotube and spinel ferrite based nanocomposites.

No.	Shielding material	Frequency band	Optimum thickness	Effect of shielding	Ref.
1.	MWCNTs/Fe ₃ O ₄ /Ti ₃ C ₂ T _x	8–18 GHz	52 μ m	49 dB	[94]
2.	Ti ₃ C ₂ /Co _{0.7} Zn _{0.3} Fe ₂ O ₄ /MWCNT	8.2–12.4 GHz	2.5 mm	83.7 dB	[95]

wave absorption capabilities. The unique structure, interfacial polarization, dielectric loss, magnetic loss, and impedance matching were all related with better EM absorption properties.

P. Yin et al.^[92] created a hybrid of (Zn_{0.5}Co_{0.5}Fe₂O₄/Mn_{0.5}Ni_{0.5}Fe₂O₄)@C-MWCNTs to improve EM wave absorption properties. A simple two-step solvothermal approach was used to create this composite structure. At a thickness of 5 mm, the maximum RL was -35.14 dB, with an effective absorption bandwidth of 0.74 GHz. The high-performance EM wave absorption

feature was linked to the synergistic impact of magnetic and dielectric loss, excellent impedance matching circumstances, and high attenuation qualities.

6. MXene, carbon nanotube and spinel ferrite based nanocomposites

MXene has recently been identified as a typical representative 2D material with excellent electrical conductivity for substantial electromagnetic wave attenuation.^[93] Nonetheless, various problems continue to impede

MXene's use. The EMI shielding capability across a broad bandwidth is insufficient, and this is also owing to high electrical conductivity, which causes a considerable reflection loss in the shielding mechanism, resulting in unwanted secondary electromagnetic pollution. MXene is used in conjunction with magnetic spinel ferrite and carbon nanotubes to address these issues (Table 7). Huguang Liu et al.,^[94] for example, reported broadband EMI shielding characteristics of MWCNTs/Fe₃O₄/

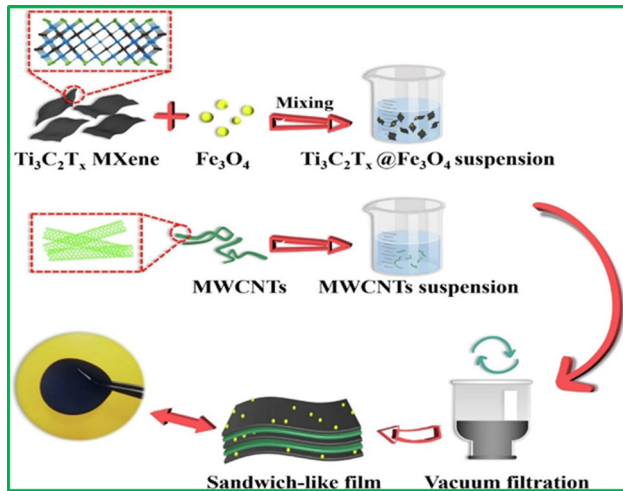


Figure 19. Schematic diagram of the composite film preparation process. Reproduced with permission from Ref. [94]. Copyright 2022. Elsevier Publication.

$Ti_3C_2T_x$ MXene multi-layer films. This study team used ultrasonic compounding and layer-by-layer vacuum-assisted filtering to create a MWCNTs/Fe₃O₄/Ti₃C₂T_x MXene composite film, as shown in Figure 19. MFT7 was assigned to the composite film made of 4-layer Fe₃O₄/Ti₃C₂T_x MXene and 3-layer MWCNTs for convenience, whereas MFT11, MFT15, and MFT19 were assigned to the 11, 15, and 19-layer composite films, respectively. As shown in Figure 20, the created composite film MFT19 has an EMI SE of 49 dB in both the X and Ku bands. When an EM wave interacts with a composite film containing a large number of mobile charge carriers, a portion of the EM wave is promptly reflected, while the remainder goes within the formed composite film for further attenuation, as shown in Figure 21. The introduction of Fe₃O₄ magnetic nanoparticles significantly reduced the impedance mismatch between the composite film and air, improving magnetic loss even more. The created multilayer design lengthened the transmission route of EM waves inside it and produced a dense conductive network, resulting in interfacial polarization and ohmic loss.

Sumit Kumar et al.^[95] have looked into the EMI shielding properties of MXene-based heterostructure composites filled with ferrites and MWCNTs. This study team used a sol-gel technique to create Ni_{0.7}Zn_{0.3}Fe₂O₄ (NZFO) and Co_{0.7}Zn_{0.3}Fe₂O₄ (CZFO) ferrite

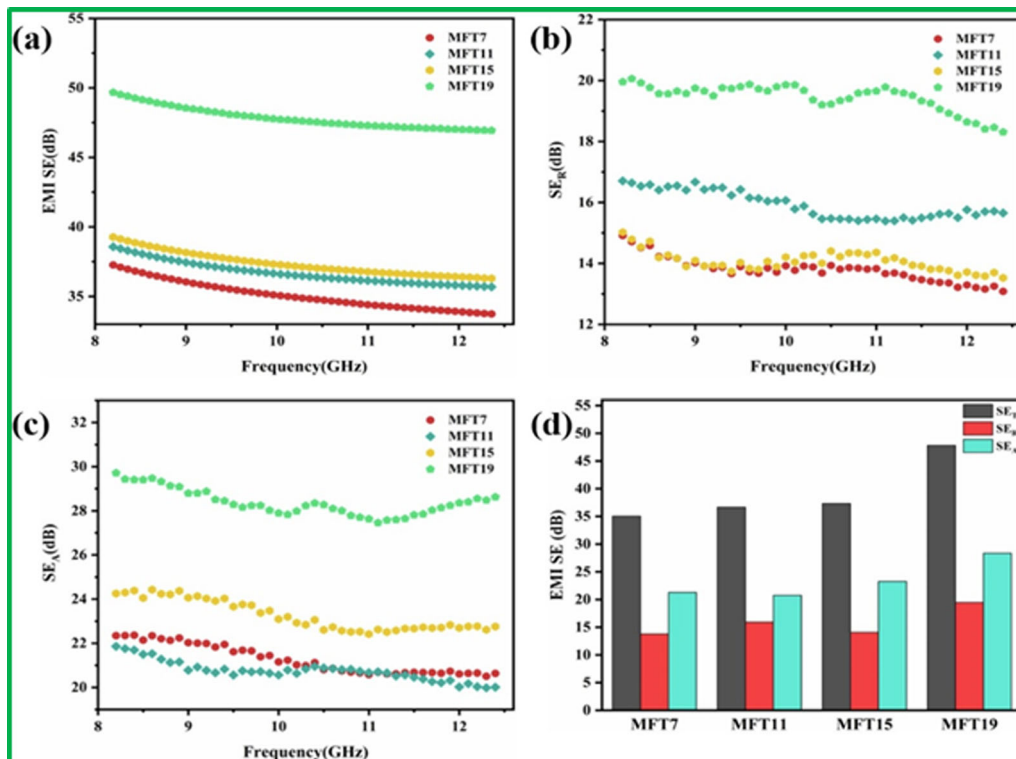


Figure 20. (a-c) EMI SE_T, SE_R, and SE_A of the composite films in the X-band. (d) Average EMI SE of the composite films in the X-band. Reproduced with permission from Ref. [94]. Copyright 2022. Elsevier Publication.

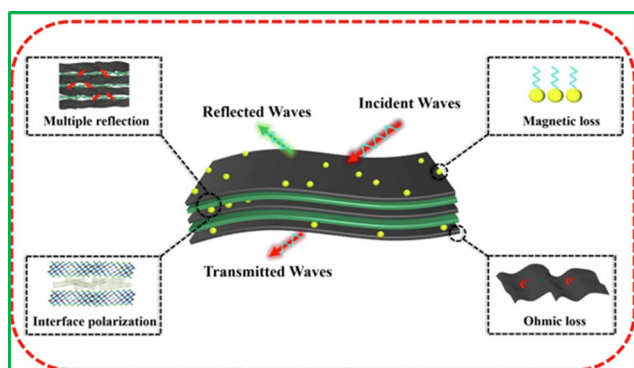


Figure 21. Schematic diagram of EMI shielding mechanism of the composite films. Reproduced with permission from Ref. [94]. Copyright 2022. Elsevier Publication.

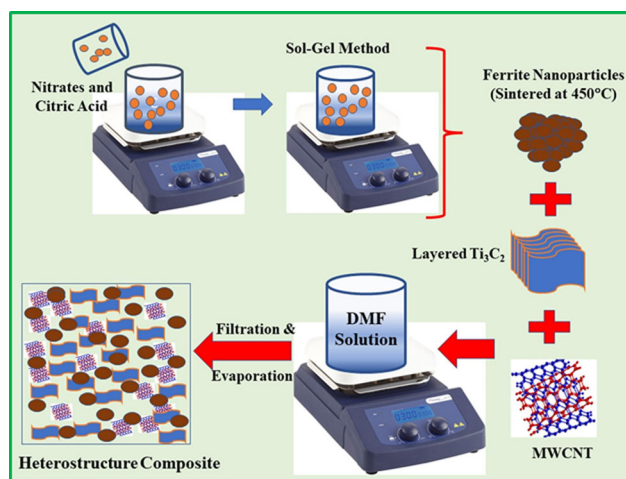


Figure 22. Schematic idea for production of ferrite nanoparticles *via* sol-gel method and fabrication of heterostructure composites *via* chemical route. Reproduced with permission from Ref. [95]. Copyright 2022. Elsevier Publication.

nanoparticles, which were subsequently chemically mixed with $\text{Ti}_3\text{C}_2\text{T}_x$ MXene and MWCNTs, as shown in Figure 22. The created $\text{Ti}_3\text{C}_2/\text{Co}_{0.7}\text{Zn}_{0.3}\text{Fe}_2\text{O}_4/\text{MWCNT}$ composite has a high SE of 83.7 dB, which was attributed to its hybrid structure, high conductivity, and strong magnetic properties (Figure 23). Because of the presence of two-dimensional conductive Ti_3C_2 and MWCNTs, the produced composites had a high conductivity due to the formation of hybrid dissipative networks and the development of extra charge carriers. The incorporation of ferrite nanoparticles into MXene layers and MWCNTs increases the dielectric and magnetic losses, which cause substantial radiation attenuation.

7. Doped carbon nanotubes and spinel ferrite based nanocomposites

Nitrogen doping in MWCNTs may improve defect/dipole polarization and dielectric loss properties, and a

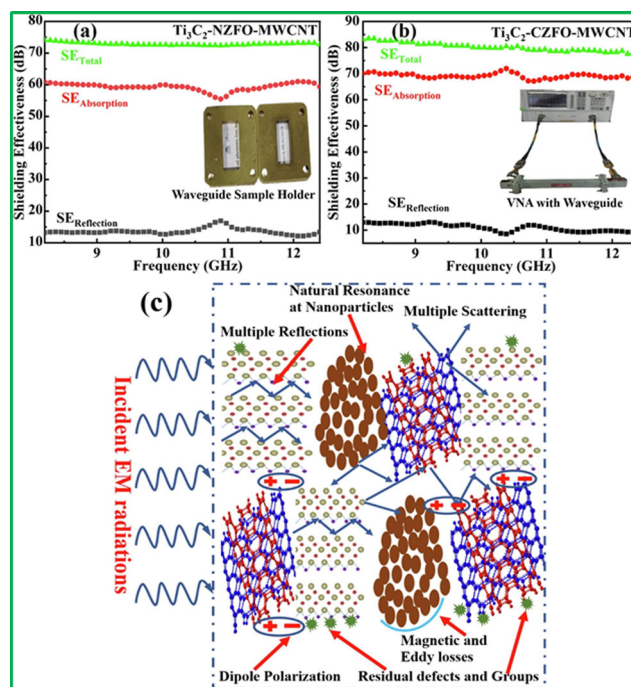


Figure 23. Frequency-dependent shielding effectiveness (a & b) consisting due to reflection and absorption for the composite samples along with the shielding mechanism (shown in c) in the 8.2–12.4 GHz frequency range. Reproduced with permission from Ref. [95]. Copyright 2022. Elsevier Publication.

high-performance EM wave absorber composite made of nitrogen-doped MWCNTs and spinel ferrite could be created.^[96–99] For example, Ruiwen Shu et al.^[100] examined the EM wave absorption properties of nitrogen-doped multi-walled carbon nanotubes/cobalt-zinc ferrite hybrid composites (NMWCNTs/ $\text{Co}_{0.5}\text{Zn}_{0.5}\text{Fe}_2\text{O}_4$). A straightforward solvothermal technique was used to create NMWCNTs/ $\text{Co}_{0.5}\text{Zn}_{0.5}\text{Fe}_2\text{O}_4$ composite structures (Figure 24). These NMWCNTs/ $\text{Co}_{0.5}\text{Zn}_{0.5}\text{Fe}_2\text{O}_4$ hybrid composites with varying NMWCNT concentrations were designated as S1 (0 mg), S2 (10 mg), and S3 (20 mg), respectively. The proposed hybrid composites demonstrated strong EM wave absorption qualities, with an RL_{\min} of -64.7 dB at 3.1 mm thickness and an effective absorption bandwidth (EAB) of 4.3 GHz at 2.1 mm thickness (Figure 25, Table 8). Amazingly, by modifying the appropriate thicknesses of absorbers, the RL_{\min} , that corresponds to the maximum microwave absorption, could be located at different frequencies. As shown in Figure 26, various EM wave absorption processes of created hybrid composites were presented, which were related with the synergistic impact of conduction loss, dielectric loss, and magnetic loss. Furthermore, nitrogen doping in MWCNTs enhanced defects and dipole polarization loss capacity while also optimizing impedance matching.

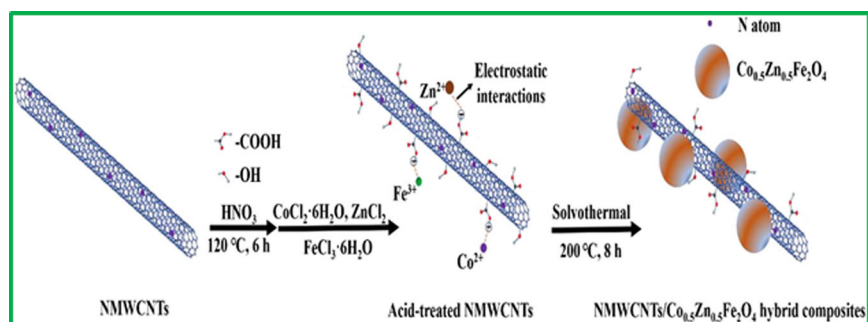


Figure 24. Schematic illustration of the synthesis process of NMWCNTs/Co_{0.5}Zn_{0.5}Fe₂O₄ hybrid composites. Reproduced with permission from Ref. [100]. Copyright 2019. Elsevier Publication.

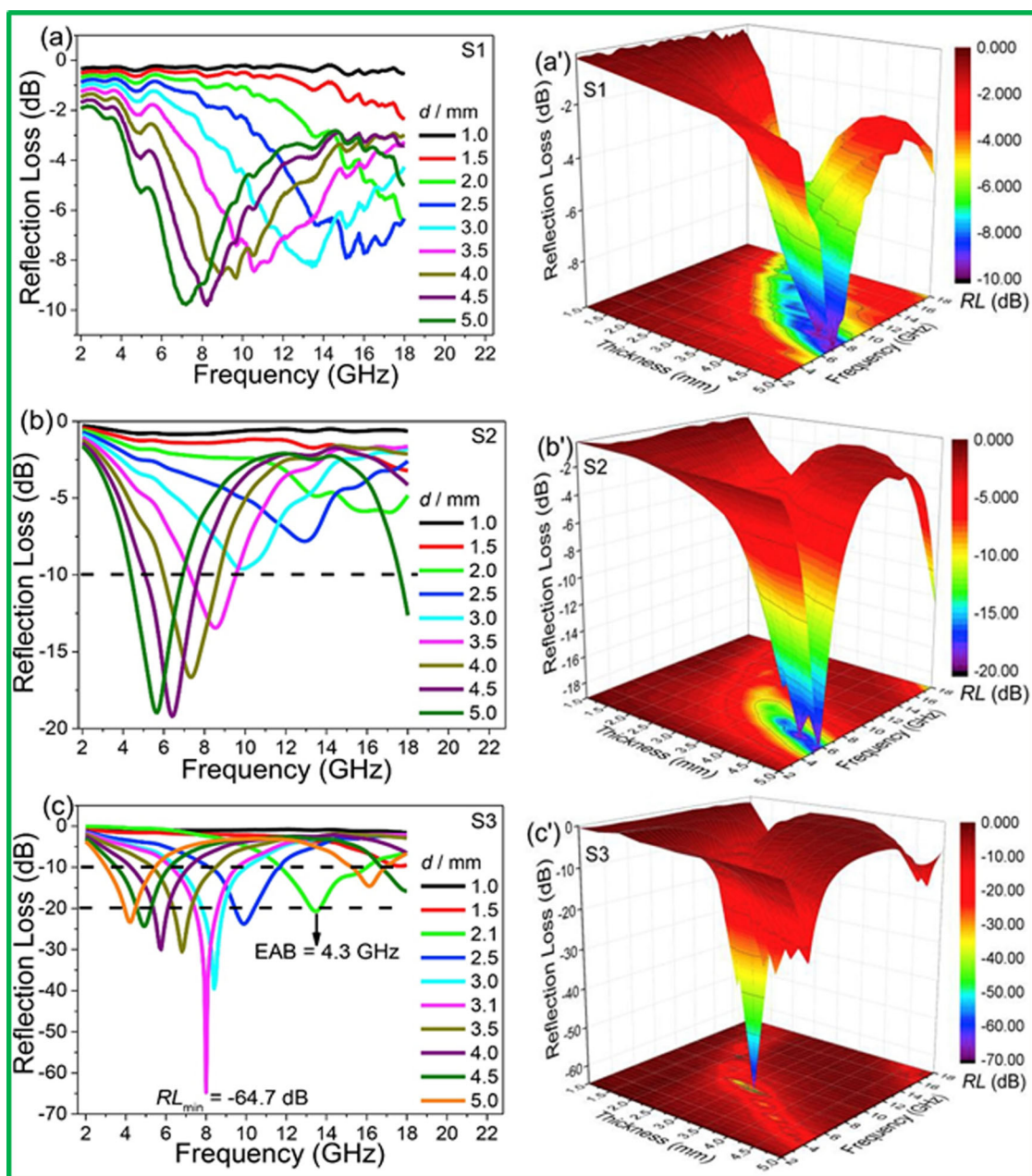
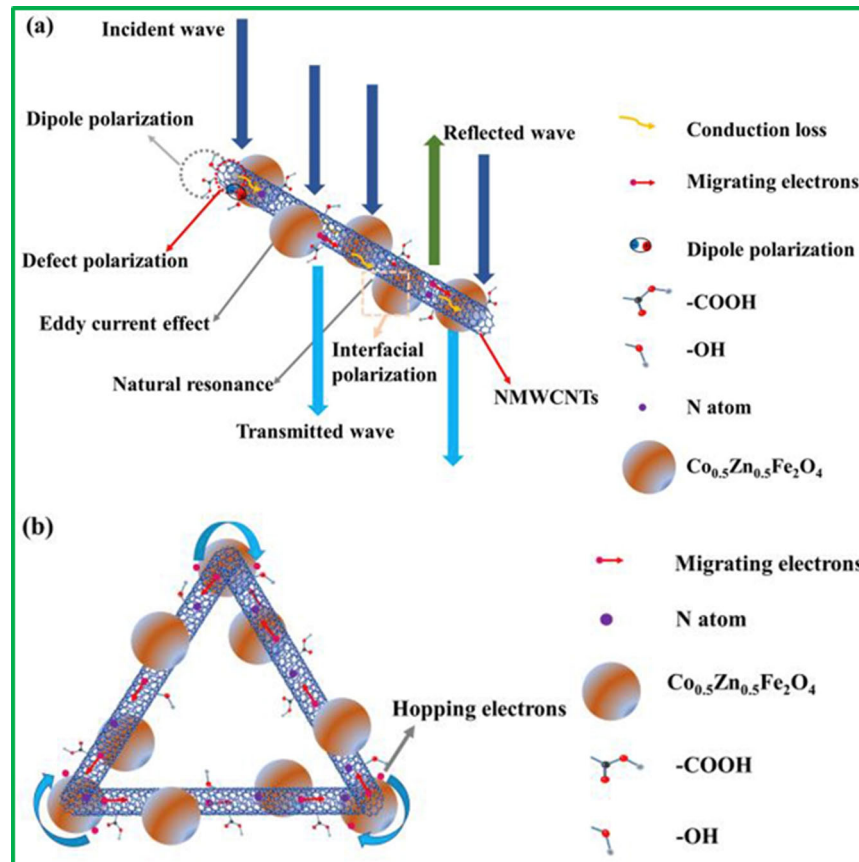


Figure 25. Frequency dependence of reflection loss with different thicknesses and 3D plots: (a) and (a') S1, (b) and (b') S2, and (c) and (c') S3. Reproduced with permission from Ref. [100]. Copyright 2019. Elsevier Publication.

Table 8. Summary of recent progress on doped carbon nanotubes and spinel ferrite based nanocomposites.

No.	Shielding material	Frequency band	Optimum thickness	Effect of shielding	Ref.
1.	NMWCNTs/Co _{0.5} Zn _{0.5} Fe ₂ O ₄	2–18 GHz	3.1 mm	–64.7 dB	[100]

**Figure 26.** Schematic illustration of the possible microwave absorption mechanisms of NMWCNTs/Co_{0.5}Zn_{0.5}Fe₂O₄ hybrid composites. Reproduced with permission from Ref. [100]. Copyright 2019. Elsevier Publication.**Table 9.** Summary of recent progress on coated carbon nanotubes and spinel ferrite based nanocomposites.

No.	Shielding material	Frequency band	Optimum thickness	Effect of shielding	Ref.
1.	nano-Fe ₃ O ₄ compact-coated CNTs	2–18 GHz	1.5 mm	–43 dB	[101]
2.	CNT-NiFe ₂ O ₄ @MnO ₂	2–18 GHz	2.5 mm	–17 dB	[102]
3.	CuS/CoFe ₂ O ₄ /MWCNT	2–18 GHz	4.64 mm	–58.74 dB	[103]

8. Coated carbon nanotubes and spinel ferrite based nanocomposites

CNTs' EM wave absorption properties may be enhanced by covering their surfaces with magnetic nanoparticles (Table 9). Na Li et al.,^[101] for example, evaluated the effect of magnetic coating on microwave absorption performance. A simple solvothermal approach was used to create two kinds of samples: nano-Fe₃O₄ compact-coated CNTs (FCCs) and Fe₃O₄ loose-coated CNTs (FLCs). The FCCs have much superior microwave absorption characteristics than the FLCs. The RL_{min} value was –43 dB at 1.5 mm thickness and an effective frequency bandwidth of up to 8.5 GHz for FCCs with a CNT to Fe³⁺ mass ratio

of 1:4 at 1.75 mm thickness. The generated FCC sample's high-performance EM wave absorption properties were related to the following dielectric relaxation process and the improved magnetic loss. As a result, the link between structure and electromagnetic parameters is important in the creation of CNT-based nanocomposite materials with high-performance EM wave absorption capabilities.

The aggregation of magnetic and dielectric nanoparticles on carbon nanotubes offers a method for improving EM wave absorption. Huifang Pang et al.,^[102] for example, evaluated the high-performance EM wave absorption properties of a hierarchical multi-layered CNT-NiFe₂O₄@MnO₂ composite. The

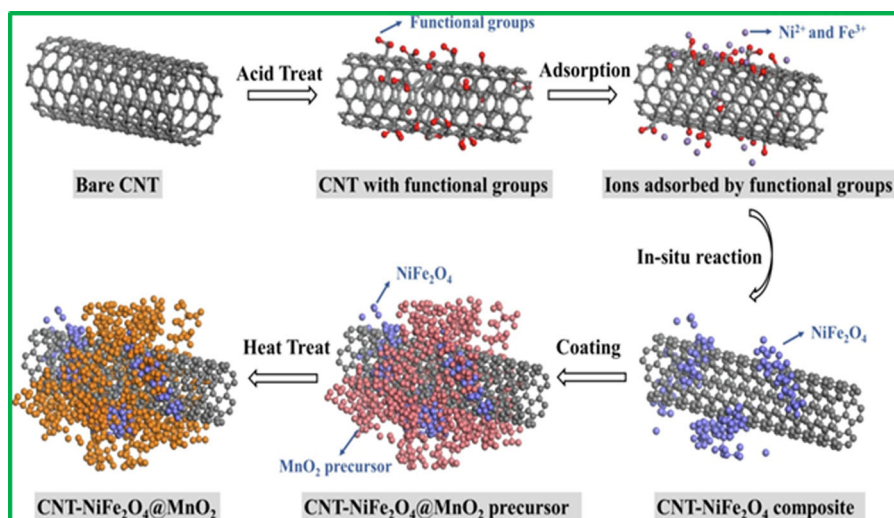


Figure 27. Illustration of the synthesis of CNT-NiFe₂O₄@MnO₂ composites. Reproduced with permission from Ref. [102]. Copyright 2022. Elsevier Publication.

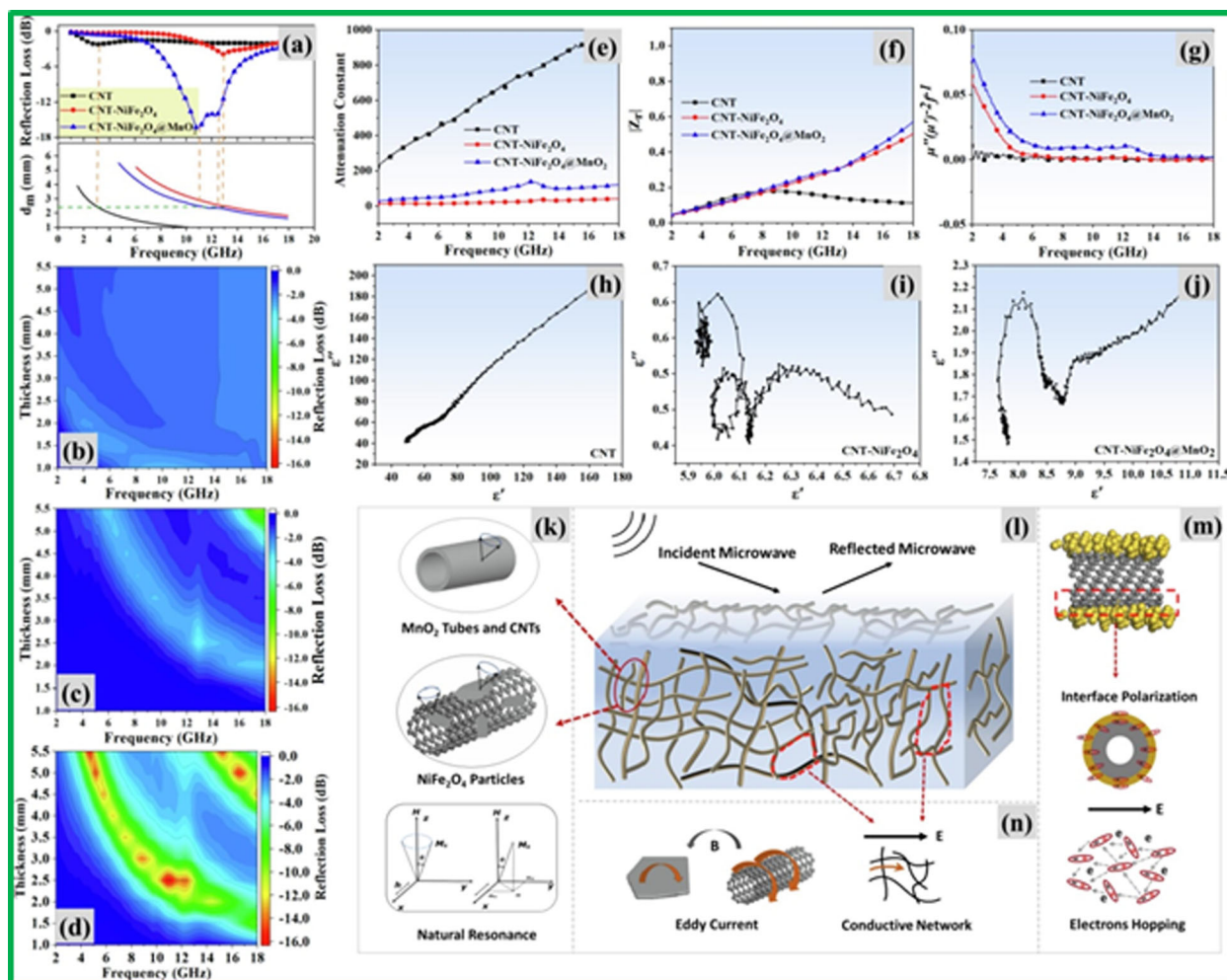
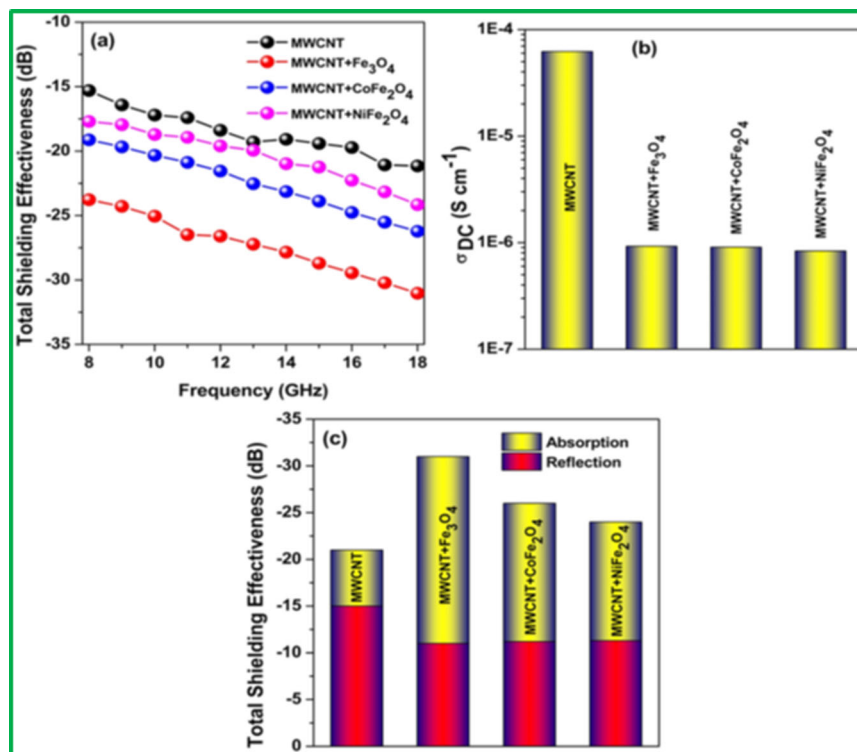


Figure 28. (a) Quarter-wavelength matching model for three materials. Reflection loss for (b) pure CNTs, (c) CNT-NiFe₂O₄, and (d) CNT-NiFe₂O₄@MnO₂ for different absorber thicknesses in the 1–5.5 mm range. The frequency dependency curves of (e) attenuation constant, (f) modulus of normalized impedance, and (g). The typical Cole-Cole semicircles for (h) pure CNT, (i) CNT-NiFe₂O₄, and (j) CNT-NiFe₂O₄@MnO₂. Schematic representation of possible attenuation mechanisms in CNT-NiFe₂O₄@MnO₂ nanomaterials: (k) Natural resonance for CNTs, MnO₂ coating, and NiFe₂O₄ particles, (l) illustration of microwave impinging CNTs-NiFe₂O₄@MnO₂ coating, (m) dielectric polarization, and (n) conductive loss induced by the electric and magnetic field. Reproduced with permission from Ref. [102]. Copyright 2022. Elsevier Publication.

Table 10. Summary of recent progress on polymer, carbon nanotube, and spinel ferrite based nanocomposites.

No.	Shielding material	Frequency band	Optimum thickness	Effect of shielding	Ref.
1.	(PDMS)/CeFe ₂ O ₄ /MWCNTs	0.5–18 GHz	–	–47 dB	[108]
2.	polycarbonate / MWNTs /Fe ₃ O ₄ @C	2–18 GHz	1 mm	–41.3 dB	[109]
3.	CoFe ₂ O ₄ /CNTs/WPU	2–18 GHz	6.8 mm	–45.8 dB	[110]
4.	TPU/Ti ₃ C ₂ T _x /MnFe ₂ O ₄ /MWCNTs	8.2–12.4 GHz	2.1 mm	31.2 dB	[111]

**Figure 29.** (a) SE_T, (b) dc electrical conductivity, and (c) absorption, and reflection part at 18GHz of various blends. Reproduced with permission from Ref. [107]. Copyright 2018, ACS Publication.

CNTs-NiFe₂O₄@MnO₂ composites were made up of hierarchical multi-layered microstructures that were created using a two-step chemical deposition process and then heat treated at 200 °C (Figure 27). NiFe₂O₄ spinel ferrite nanoparticles were initially precipitated on CNT surfaces before being uniformly coated by a MnO₂ layer. When compared to CNTs and CNT-NiFe₂O₄ composite systems, the CNT-NiFe₂O₄@MnO₂ composite system had an RL = -17 dB and an effective absorption bandwidth of 3.8 GHz (Figure 28). The created composites benefited from both magnetic and dielectric components. The presence of dielectric and magnetic elements on CNTs improved impedance matching, dielectric attenuation, and magnetic attenuation. The quarter-wavelength matching model was satisfied by all samples, as shown in Figure 28. By means of a geometric effect, the composites as prepared attenuated electromagnetic waves. The counter-balance of incident and reflected microwave also contributed to absorption when the phase difference between the air-absorber and absorber-metal interface

was 180°. It was intriguing to note that the CNT-NiFe₂O₄@MnO₂ had two RL peaks in the range of 2 to 18 GHz, which significantly contributed to the absorption bandwidth. The quarter-wavelength matching model states that if the electromagnetic parameter (μ and ϵ) is increased properly, it may result in the two-peaks curve of RL in the frequency range of 2–18 GHz.

Xinyang Wang et al.^[103] also looked into the effect of copper sulfide nanosphere shells on the EM wave absorption characteristics of cobalt ferrite/carbon nanotube composites. CuS adherence to the CoFe₂O₄/MWCNT binary composite was shown to improve EM wave attenuation capability. However, since the impedance matching level was reduced, EM wave absorption properties may be modified by varying the number of CuS nanoparticles. At 1.77 mm matching thickness, the CuS/CoFe₂O₄/MWCNT composite had a maximum EM wave absorption bandwidth of 5.26 GHz. At 4.64 mm matching thickness, this designed composite system has a minimum RL of -58.74 dB.

9. Polymer, carbon nanotube, and spinel ferrite based nanocomposites

Lightweight and flexible polymer-based nanocomposites as EM wave absorber materials have recently garnered a lot of interest due to numerous additional advantages such as corrosion protection, large-area manufacturing, cheap cost, and so on.^[104,105] Polymer-based nanocomposites containing dielectric and magnetic fillers have the potential to be extremely

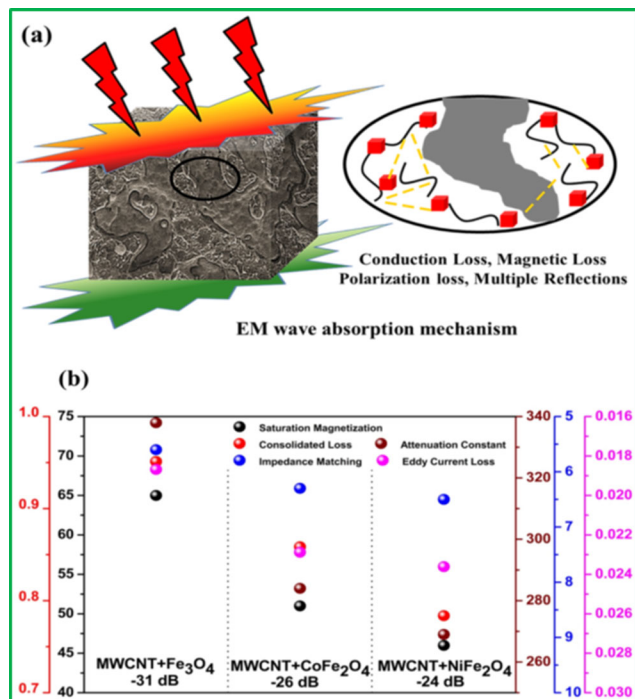


Figure 30. (a) Schematic representation of the shielding mechanism through the synergistic contribution of both filler nanomaterials and (b) characteristic parameters for effective shielding of different blends containing different types of ferrite particles along with the MWCNTs. Reproduced with permission from Ref. [107]. Copyright 2018, ACS Publication.

efficient EM wave absorber materials (Table 10).^[106] For example, Sourav Biswas et al.^[107] used a biphasic co-continuous mix of polycarbonate and polyvinylidene fluoride (PC/PVDF) as the matrix and combined it with conducting multiwalled carbon nanotubes (MWCNTs) and magnetic inverse-spinel ferrites, MFe₂O₄ (M = Fe, Co, Ni) phases. All of the nanoparticles were mixed with the blend components, and an appropriate surface functionalization technique was used to compel the nanoparticles to localize in the different blend components. A one-pot hydrothermal synthesis technique was used to create ferrite nanoparticles such as Fe₃O₄, CoFe₂O₄, and NiFe₂O₄. A melt compounder was used to create polymer blends comprising PC/PVDF and filler nanoparticles. As shown in Figure 29, the total shielding effectiveness (SE_T) ranged from -21 dB to -31 dB with different kinds of spinel ferrite nanoparticle fillers in the presence of MWCNTs. When ferrite nanoparticles were combined with MWCNTs, the dc conductivity decreased. It was discovered that the addition of ferrites to MWCNTs resulted in shielding *via* absorption rather than reflection. Furthermore, it was found that the synergistic contribution of both conducting and magnetic nanoparticles is significant for improving overall shielding efficacy through absorption, as shown in Figure 30. The shielding efficiency of ferrite nanoparticles is controlled by their interactions with incoming microwave radiation. In the developed blends, Fe₃O₄ displayed the highest shielding efficacy, which was attributable to high saturation magnetization, high consolidated loss parameters, high attenuation constant, superior impedance matching, and reduced eddy current losses.

Xiaojun Chen et al.^[108] also explored the microwave absorption properties of polydimethylsiloxane (PDMS)/CeFe₂O₄/MWCNTs nanocomposites. The

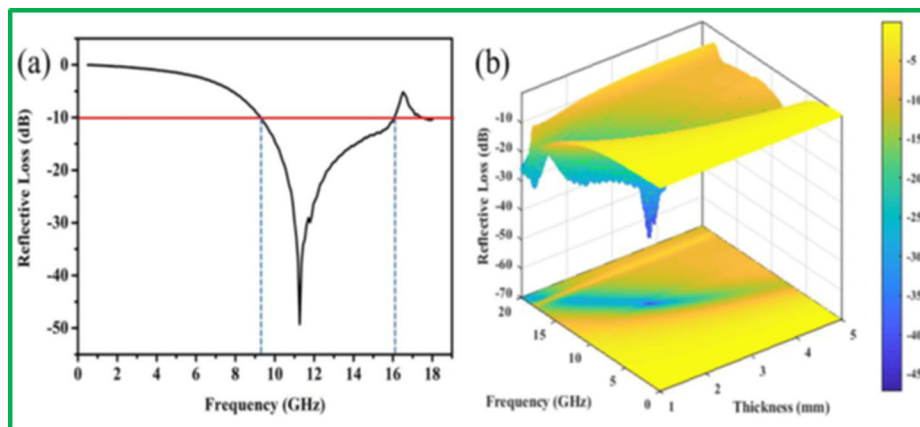


Figure 31. Reflective loss (a) and 3D map reflective loss (b) of PDMS/CeFe₂O₄/MWCNTs. Reproduced with permission from Ref. [108]. Copyright 2022. Elsevier Publication.

greatest reflecting loss was -47 dB at 11.3 GHz with an effective absorption bandwidth of 6.9 GHz for the PDMS/CeFe₂O₄/MWCNTs coating with a mass ratio of 5:1 (CeFe₂O₄/MWCNTs:PDMS) (Figure 31). Additionally, it was observed that, in accordance with the theory of the quarter wavelength, the maximum loss peak gradually decreases as the sample thickness

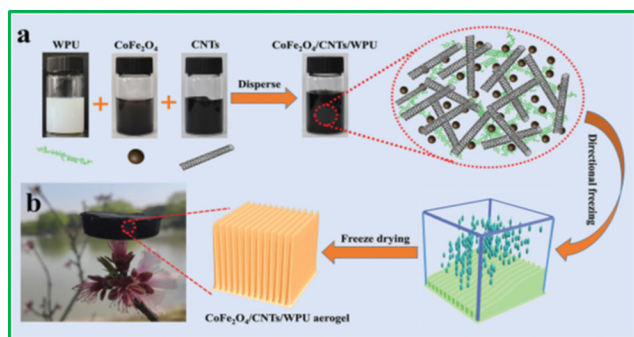


Figure 32. (a) Schematic diagram of the synthesis process of CoFe₂O₄/CNTs/WPU hybrid aerogels, (b) CCW-3 aerogel on top of the stamen. Reproduced with permission from Ref. [110]. Copyright 2021, RSC Publication.

increases. Shital P. Pawar et al.^[109] discovered effective microwave absorption with a wide bandwidth for polycarbonate composites including MWNTs and “brick-like” lossy magnetic Fe₃O₄ nanoparticles encapsulated in carbon (Fe₃O₄@C). At a thickness of 1 mm, the produced nanocomposites demonstrated an excellent RL of -41.3 dB at 17.7 GHz and a remarkable bandwidth of 4.4 GHz. Furthermore, Jiawei Luo et al.^[110] examined the microwave absorption properties of hybrid cobalt ferrite (CoFe₂O₄)/carbon nanotubes (CNTs)/waterborne polyurethane (WPU) aerogels. A simple directional freeze-drying procedure was used to create the CoFe₂O₄/CNTs/WPU hybrid (CCW) aerogels (Figure 32). CNTs and WPU were used as the skeleton and crosslinker, respectively, to create a porous framework in this produced hybrid aerogel, and CoFe₂O₄ nanoparticles were evenly inserted inside this system. The generated aerogels were labeled CCW-1, CCW-2, and CCW-3 based on the quantity of CNTs added (0.15, 0.3, and 0.45 g, respectively). The hybrid aerogels’ optimal microwave absorption characteristic was -45.8 dB at 11.68 GHz

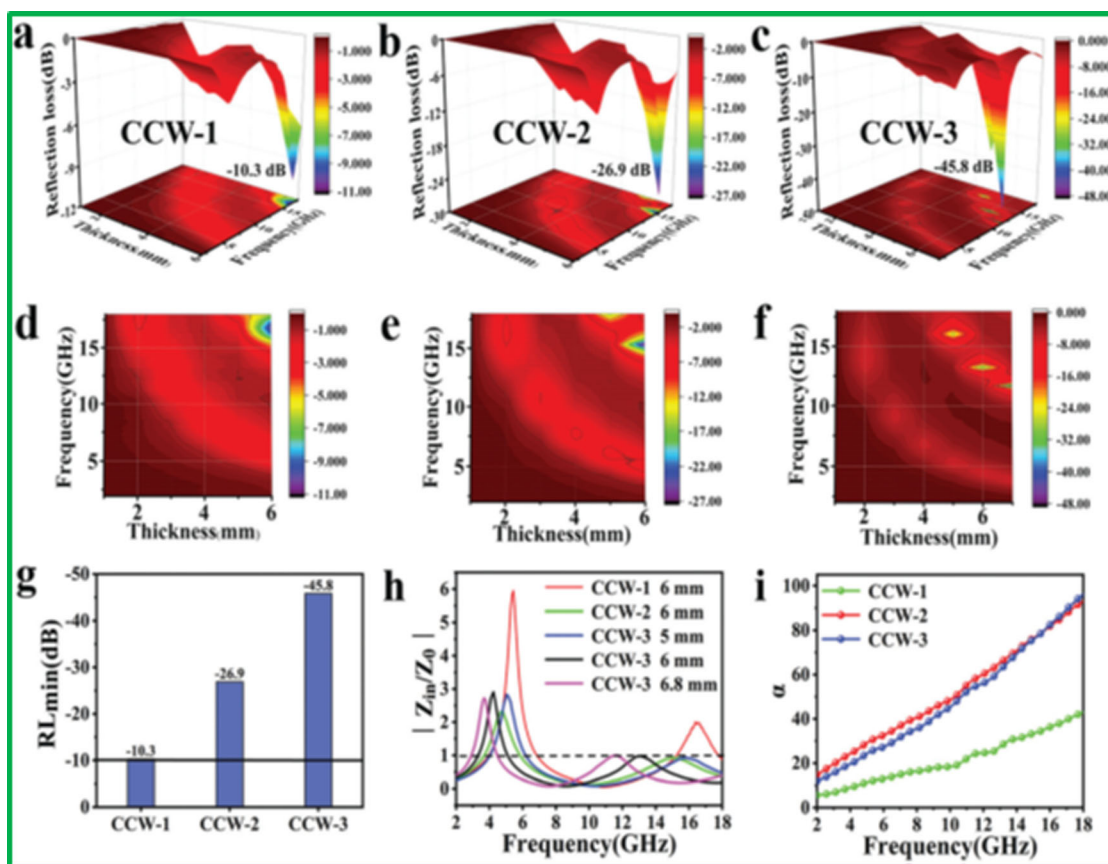


Figure 33. Correlation between the reflection loss and frequency of the samples *via* 3D contour maps of CCW-1 (a), CCW-2 (b), CCW-3 (c). (d–f) Corresponding 2D contour maps of the reflection loss values of the CCW aerogels. (g) Minimum reflection loss of CCW-1, CCW-2, and CCW-3 aerogels, respectively. (h) Corresponding thickness of the samples with their optimum impedance matching values ($|Z_{in}/Z_0|$). (i) Curves of the attenuation constant. Reproduced with permission from Ref. [110]. Copyright 2021, RSC Publication.

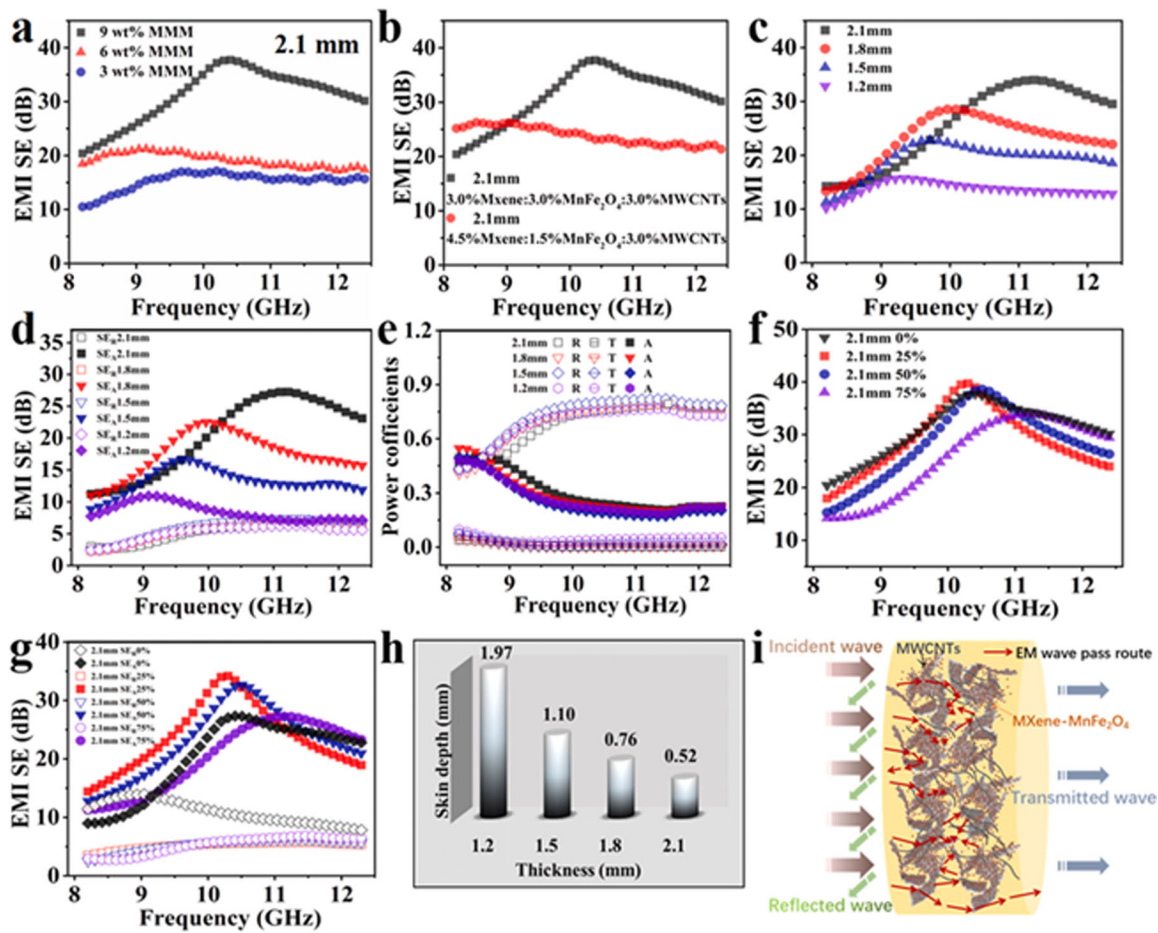


Figure 34. SE_T of TMMM composites with 0% porosity and different MMM filler contents (a); SE_T of TMMM composites with different Mxene and $MnFe_2O_4$ mass ratio (b); SE_T , SE_A , and SE_R of TMMM composites with 75% porosity and various thicknesses (c, d); Power coefficients (A, T, and R) as a function of frequency at 75% porosity (e); SE_T , SE_A and SE_R of TMMM composites with different porosity at fixed thickness of 2.1 mm (f, g); Skin depth as a function of thickness at 75% porosity (h); Diagram of the EM waves shielding mechanism of TMMM composites (i). Reproduced with permission from Ref. [111]. Copyright 2022. Elsevier Publication.

with a matching thickness of 6.8 mm (Figure 33). It was discovered that the CCW-3 aerogel has an impedance near to one as well as an excellent attenuation ability. In addition, the RL_{min} of the CCW-3 aerogel reached a higher level of -45.8 dB even though the attenuation constant of the CCW-2 aerogel was very similar to that of the CCW-3 aerogel. This phenomenon is caused by the CCW-3 aerogel's impedance, which could reach 1, while also having ideal attenuation capabilities.

Thermoplastic polyurethane (TPU)/ $Ti_3C_2T_x$ (MXene)/ $MnFe_2O_4$ /Multi-walled carbon nanotubes (MWCNTs) (i.e., TMMM) composites with different pore sizes and porosity by fused deposition molding (FDM) printing were reported by Zhongming Li et al.^[111] The increase of nanofiller led to an improvement in EMI shielding performance (Figure 34). The 2.1 mm-thick printed composite's average electromagnetic interference shielding efficiency (EMI SE) value

was 31.2 dB, which indicates that 99.9242% of electromagnetic waves can be shielded. The SE_A , which varied in thickness and porosity, all contributed more to the SE_T than the SE_R , indicating that the absorption mechanism played a more significant role in the entry of EM waves than the reflection mechanism. Additionally, due to the impedance mismatch at the interface brought on by the high conductivity of the composite, R rises significantly with thickness. It was important to note that SE_A is higher than SE_R and that R was higher than A almost throughout the entire frequency range. These results demonstrated the distinction between SE_A and SE_R , which represented the EM wave entering the composites, and A and R, which were quantitative characteristics of the entire incident EM wave on the composites. Because reflection happens before absorption, the EM wave shielding mechanism of the TMMM composite was dominated by reflection. As soon as the EM waves

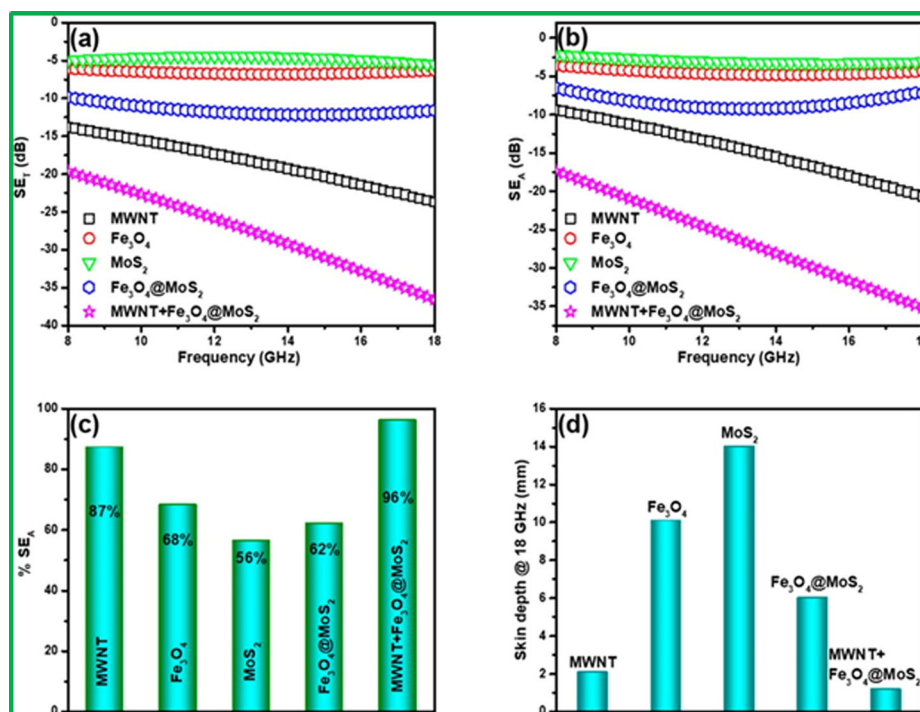


Figure 35. (a) Total shielding effectiveness, (b) shielding effectiveness due to absorption, (c) % shielding effectiveness due to absorption and reflection, and (d) skin depth of the composites. Reproduced with permission from Ref. [113]. Copyright 2019, ACS Publication.

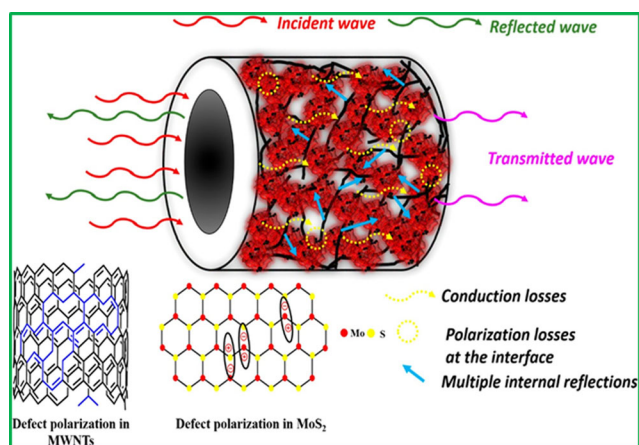


Figure 36. Mechanism of EMI Shielding in PU-Dopa Composites. Reproduced with permission from Ref. [113]. Copyright 2019, ACS Publication.

reached the composite material, absorption took command of the shielding mechanism.^[112] In addition, the skin depth decreased dramatically as the composite's thickness increased. Due to the impedance mismatch between the two different media, a significant amount of EM waves was reflected when they came into contact with the front interface between the TMMM and air space. Because the conductive fillers used in MMM multidimensional hybridization

repeatedly reflected and absorbed electromagnetic waves, the non-reflected wave propagated to the material's interior and experienced an exponential decline in intensity. When the EM wave arrived at the back interface, some of the EM wave passed through the shielding materials while the EM wave that entered had mechanisms that were dominated by absorption.

10. Semiconducting nanoparticles, carbon nanotubes, and spinel ferrite based nanocomposites

Electric dipoles derived from semiconducting nanoparticles, magnetic dipoles derived from magnetic spinel ferrite, and electrical conductivity derived from carbon nanotubes may all exhibit high-performance EM wave absorption properties. Recently, MoS₂ has been shown to be helpful for EMI shielding as a 2D layered material with some intriguing electrical properties. The existence of mobile charge carriers in MoS₂ may interact with the electric component of EM waves, resulting in attenuation of incoming EM waves. A. V. Menon et al.^[113] looked into the EMI shielding properties of "mussel-inspired" dopamine functionalized polyurethane (PU) with multiwalled carbon nanotubes (MWNTs) and ferrite doped with MoS₂ (Fe₃O₄@MoS₂). Hybrid nanocomposite systems of

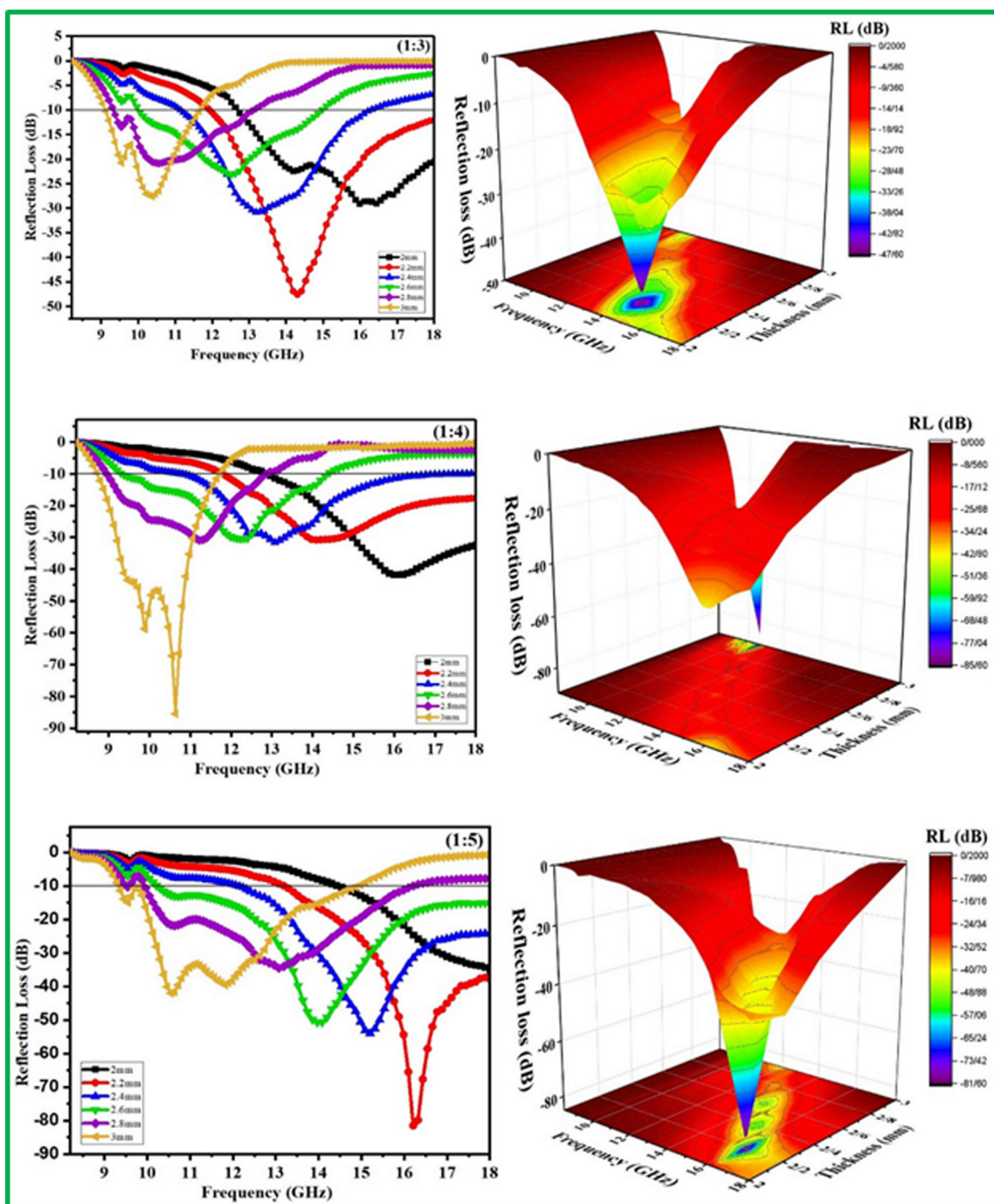


Figure 37. Reflection loss of MWCNT/CuO/Fe₃O₄/PANI (1:3), (1:4), and (1:5) versus frequency for different absorber thicknesses (2D, 3D). Reproduced with permission from Ref. [116]. Copyright 2022, Springer Nature Publication.

Fe₃O₄ and MoS₂ (Fe₃O₄@MoS₂) combined with conducting MWNTs demonstrated – 36.6 dB EMI shielding with up to 96% incident EM wave absorption (Figure 35). EMI shielding properties were linked to heterogeneous interface polarization losses, eddy current losses, numerous internal reflections from MWNTs, and polarization losses from defect sites in the nanoparticles (Figure 36). In most cases, an incident EM wave degrades as it moves further into the

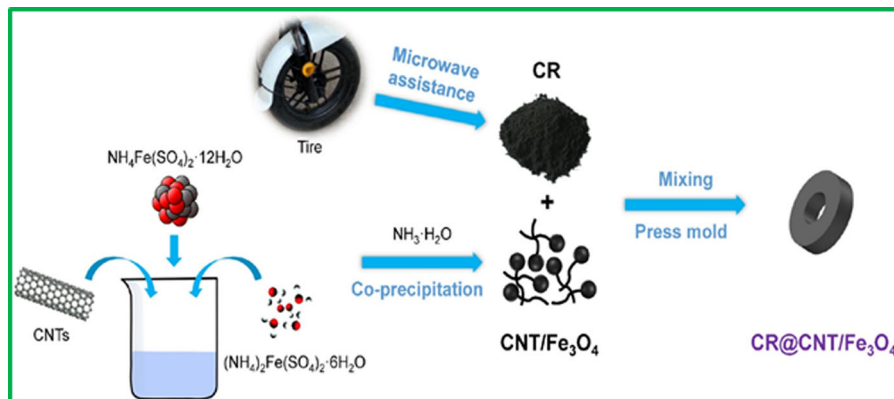
shield, and it does this by conductively fencing the wave. The skin depth of the shield is the depth that an incoming electromagnetic wave must travel through in order to be reduced in intensity by 1/e, or approximately 37%. The thickness (t), magnetic permeability (μ), and electrical conductivity (σ) of a shield determine its skin depth (δ), which is closely related to SE_A by the relation, $\delta = 1/\sqrt{\pi f \mu \sigma} = -8.68(t/SE_A)$. The skin depths of the composites

Table 11. Summary of recent progress on semiconducting nanoparticles, carbon nanotubes, and spinel ferrite based nanocomposites.

No.	Shielding material	Frequency band	Optimum thickness	Effect of shielding	Ref.
1.	PU/MWNTs/Fe ₃ O ₄ @MoS ₂	8–18 GHz	–	–36.6 dB	[113]
2.	MWCNT/CuO/Fe ₃ O ₄ /PANI	8–18 GHz	2.2 mm	–87.4 dB	[116]

Table 12. Summary of recent progress on semiconducting nanoparticles, carbon nanotubes, and spinel ferrite based nanocomposites.

No.	Shielding material	Frequency band	Optimum thickness	Effect of shielding	Ref.
1.	crumb rubber@CNT/Fe ₃ O ₄	2–18 GHz	2.3 mm	60.46 dB	[117]

**Figure 38.** The schematic diagram of fabricating CR@CNT/Fe₃O₄ composites. Reproduced with permission from Ref. [117]. Copyright 2022. Elsevier Publication.

made solely of Fe₃O₄, MoS₂, and Fe₃O₄@MoS₂ were 10.1 mm, 14 mm, and 6 mm, respectively, as predicted by the SE_A values (Figure 35). The skin depth decreased to 2.1 mm with the addition of MWNTs, and the decrease was more pronounced when MWNTs and Fe₃O₄@MoS₂ were combined in a synergistic manner, manifesting in a skin depth as low as 1.2 mm. The aforementioned findings support that the presence of a complex heterogeneous shield enhances the attenuation of EM waves, which can result in a gradual decline in the incoming EM wave's power. One of factor that could cause magnetic loss is eddy current loss, and is determined by the material's magnetic permeability (μ), frequency (f), and conductivity (σ), as follows $C_o = \mu''(\mu')^{-2}f^{-1} = \frac{2}{3} \pi\mu_0 d^2 \sigma$. It was noticed that in all frequency ranges between 8 and 18 GHz, the composites containing both MWNT and Fe₃O₄@MoS₂ exhibit eddy current losses. Additionally, the semiconducting MoS₂ and the conducting MWNTs jointly contribute to eddy current losses.

Copper oxide (CuO), a narrow-gap semiconductor, was used to create high-performance EM wave-absorbing composites.^[114,115] S.S. Afzali et al.,^[116] for example, studied the EM wave absorption characteristics of MWCNT/CuO/Fe₃O₄/Polyaniline nanocomposites. These MWCNT/CuO/Fe₃O₄/PANI nanocomposites

were created using three different weight ratios of CuO/Fe₃O₄/PANI to MWCNT (1:3, 1:4, and 1:5). As shown in Figure 37, the minimal reflection losses for MWCNT/CuO/Fe₃O₄/PANI nanocomposites with weight ratios of (1:3), (1:4), and (1:5) were 45.7, 58.7, and 85.4, 87.4 dB, respectively (Table 11). The unique construction of the quaternary MWCNT/CuO/Fe₃O₄/PANI composite with numerous interfaces and weight ratio analysis of each proposed composite system resulted in a high-performance EM wave absorber, according to this study group. Further, it was noticed that the absorber's thickness has a noteworthy impact on the microwave absorption properties. As absorbent thickness was increased, the RL_{min} peak gradually shifted to a lower frequency, and followed the formula $f_m = c/2\pi\mu''d$, where d is the sample thickness and f_m is the frequency adapted to RL_{min}.

11. Rubber, carbon nanotubes, and spinel ferrite based nanocomposites

Recycling crumb rubber (CR) may be utilized to create a unique composite that absorbs electromagnetic radiation using carbon nanotubes and spinel ferrite (Table 12). Jiajia Zheng et al.^[117] has explored the EM wave absorption properties of crumb rubber@carbon

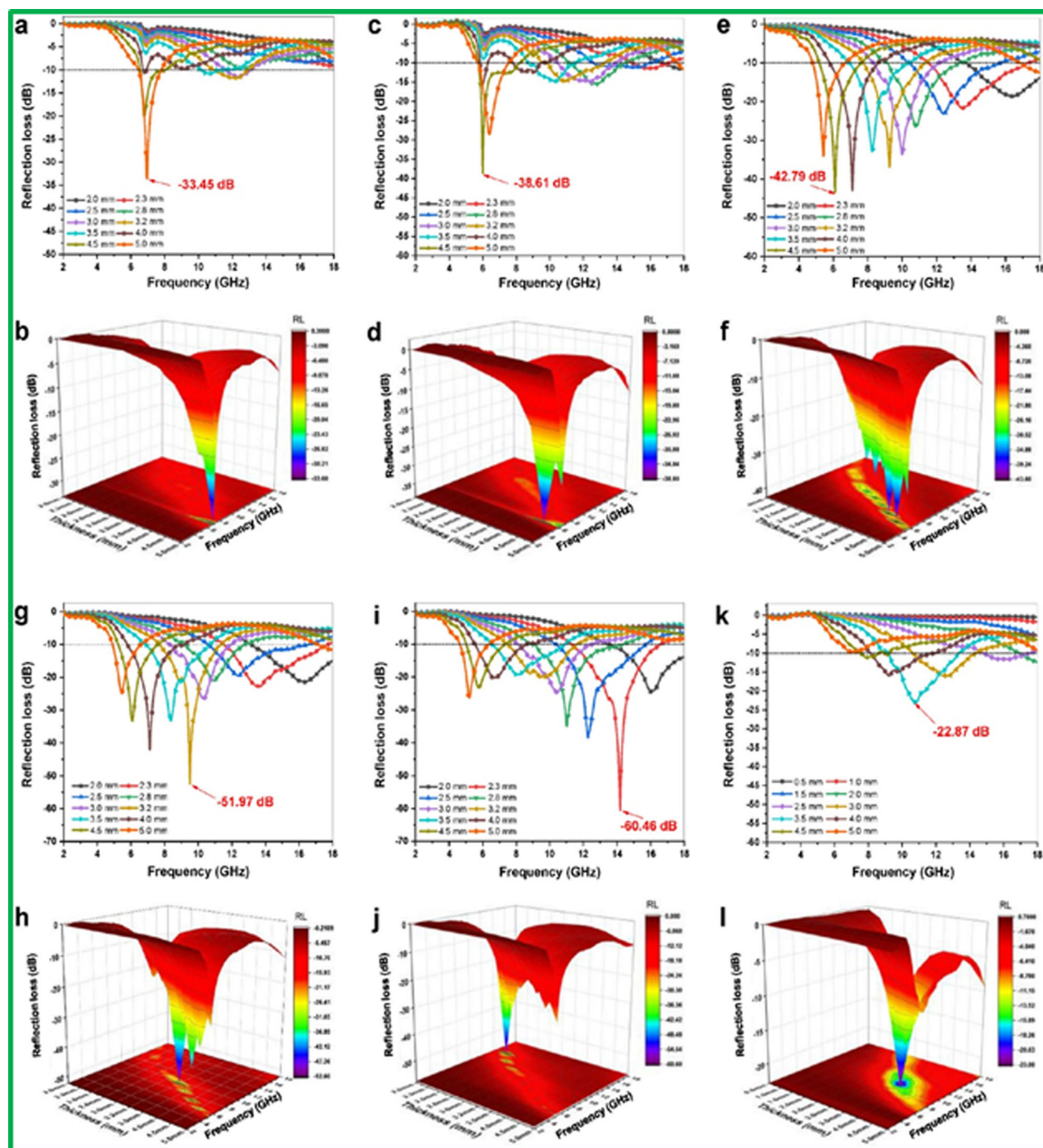


Figure 39. The RL of CR@CNT/Fe₃O₄ composites with different thicknesses and frequencies: (a, b) CR@CNT/Fe₃O₄-1:0.5, (c, d) CR@CNT/Fe₃O₄-1:1, (e, f) CR@CNT/Fe₃O₄-1:1.5, (g, h) CR@CNT/Fe₃O₄-1:2, (i, j) CR@CNT/Fe₃O₄-1:3, and (k, l) CNT/Fe₃O₄. Reproduced with permission from Ref. [117]. Copyright 2022. Elsevier Publication.

nanotube/Fe₃O₄ composites. A co-precipitation approach was used to create the CNT/Fe₃O₄ composites. Furthermore, composite systems with CR and varying CNT/Fe₃O₄ concentrations (mass ratios = 1:0.5, 1:1, 1:1.5, 1:2, and 1:3) were created (Figure 38). The resultant composite has an RL_{min} of -60.46 dB at 14.19 GHz and a thickness of 2.3 mm, as well as a

5.5 GHz effective absorption bandwidth (Figure 39). The synergy impact of coordinated dielectric and magnetic losses, efficient interface impedance matching, and internal multiple reflections were connected with high-performance EM wave absorption characteristics (Figure 40). The CR@CNT/Fe₃O₄ composite recycling from scrap tire rubber produced is a

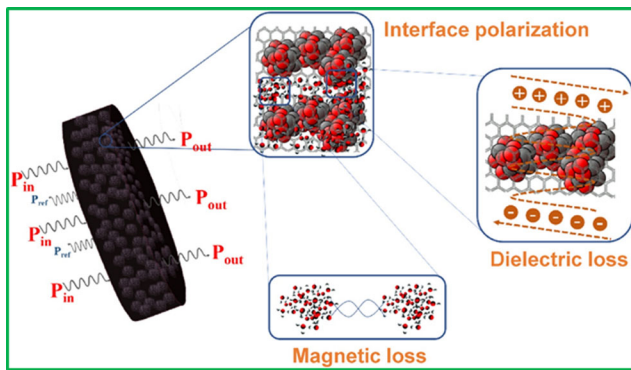


Figure 40. EMA mechanisms of CR@CNT/Fe₃O₄ composites. Reproduced with permission from Ref. [117]. Copyright 2022. Elsevier Publication.

low-cost microwave absorber for lowering both electromagnetic and black pollution.

12. Conclusion and perspective

Carbon nanotubes and spinel ferrite-based nanocomposites as EMI shielding and microwave absorbers have garnered a lot of interest from researchers and academics in recent years. We evaluated recent achievements in EMI shielding and microwave absorber nanocomposite materials of carbon nanotubes and spinel ferrites in this review paper, covering the influence of adding graphene, MXene, semiconductor particles, polymer systems, rubber, coating, doped carbon nanotubes, and so on. To develop efficient EM wave absorption materials made of carbon nanotubes and spinel ferrites, good integration of dielectric and magnetic losses is essential to get the impedance matching level as well as the high absorption properties of the composite materials. The conduction loss, dielectric loss, magnetic loss, and impedance matching of carbon nanotubes and spinel ferrite-based nanocomposites can be effectively regulated to achieve efficient attenuation and absorption of incident EM waves by sensibly controlling the components' structural and morphology characteristics, doping in components, coating, and the addition of third or fourth dielectric or magnetic components. This article also includes a discussion on lightweight, flexible, and high-performance polymer nanocomposites comprising carbon nanotubes and spinel ferrites. However, apart from these efforts on the EM wave absorption examination of carbon nanotubes and spinel ferrite-based nanocomposites, other important issues may be addressed in the future.

1. Concentrate on improving EM wave absorption via electromagnetic parameters controlled by crystal structure, particle size, and morphology.

2. Development of porous structure-based composites based on carbon nanotubes and spinel ferrites. The porous structure has a dynamic influence on EM wave attenuation because absorption occurs owing to an impedance mismatch between the pores filled with air and the many surfaces.
3. Development of diverse polymer nanocomposites including carbon nanotubes and spinel ferrites as fillers, as well as additional research into the function of filler dispersion, kinds, and contents.
4. Use of semiconductor particles as additional components, such as ZnO, TiO₂, SnO₂, MoS₂, WO₃, and others, as well as a thorough investigation of the impact of interfacial polarization.
5. Use of 2D materials containing carbon nanotubes and spinel ferrites, such as 2D nitrides (e.g., boron nitride and graphitic carbon nitride), transition metal dichalcogenides, and black phosphorus.
6. A number of important factors still need to be taken into consideration when designing advanced EMI shielding composite materials in light of the current situation, including solid mechanical properties, wide absorption frequency, broad-band absorption capacity to prevent signal detection, thermal stability behavior, antioxidation, etc.
7. To fabricate novel composites and create new opportunities to address problems in real-world applications, it is necessary to develop various engineering processing techniques, such as coatings, screen and 3D printing.
8. Fabrication of novel composites of carbon nanotubes with spinel ferrite nanoparticles can offer a workable solution with a wide range of controllable structural designs to meet the demands of real applications while simultaneously achieving efficient EMI shielding and high mechanical strength.
9. The best option for facilitating a variety of responses as microwave absorbers and opening up new avenues may be multilayer composite architectures made up of different combinations of conducting polymers, carbon nanotubes, and spinel ferrite magnetic nanoparticles.

The exploration of EM wave absorption on carbon nanotubes and spinel ferrite-based nanocomposites is currently ongoing, and there is still a lot to learn about novel nanocomposites based on these components that have good EM wave absorption capabilities. Furthermore, research on ternary and quaternary

component hybrid composites of carbon nanotubes and spinel ferrites for further improvement in EM wave absorption properties is still in its early stages. This review study, we think, provides insight into future problems and techniques for creating novel materials as next-generation EM wave absorbers.

Acknowledgment

The authors gratefully acknowledge the financial assistance provided by the Ministry of Education, Youth, and Sports of the Czech Republic-DKRVO (RP/CPS/2022/007).

Disclosure statement

No potential conflict of interest was reported by the authors.

ORCID

Raghvendra Singh Yadav  <http://orcid.org/0000-0003-1773-3596>

Ivo Kuřitka  <http://orcid.org/0000-0002-1016-5170>

References

1. Yadav, R. S.; Anju; Kuřitka, I. Spinel Ferrite and MXene-Based Magnetic Novel Nanocomposites: An Innovative High-Performance Electromagnetic Interference Shielding and Microwave Absorber. *Crit. Rev. Solid State Mater. Sci.* 2022, 1–39. doi:10.1080/10408436.2022.2067122.
2. Yadav, R. S.; Kuritka, I.; Vilcakova, J. *Advanced Spinel Ferrite Nanocomposites for Electromagnetic Interference Shielding Applications*; Elsevier: Amsterdam, 2021. <https://www.sciencedirect.com/book/9780128212905/advanced-spinel-ferrite-nano-composites-for-electromagnetic-interference-shielding-applications>.
3. Lv, H.; Yang, Z.; Pan, H.; Wu, R. Electromagnetic Absorption Materials: Current Progress and New Frontiers. *Prog. Mater. Sci.* 2022, 127, 100946. doi:10.1016/j.pmatsci.2022.100946.
4. Zhao, H.; Wang, F.; Cui, L.; Xu, X.; Han, X.; Du, Y. Composition Optimization and Microstructure Design in MOFs-Derived Magnetic Carbon-Based Microwave Absorbers: A Review. *Nano-Micro Lett.* 2021, 13, 208. doi:10.1007/s40820-021-00734-z.
5. Zhang, X.; Qiao, J.; Jiang, Y.; Wang, F.; Tian, X.; Wang, Z.; Wu, L.; Liu, W.; Liu, J. Carbon-Based MOF Derivatives: Emerging Efficient Electromagnetic Wave Absorption Agents. *Nanomicro Lett.* 2021, 13, 135. doi:10.1007/s40820-021-00658-8.
6. Zhang, Z.; Cai, Z.; Wang, Z.; Peng, Y.; Xia, L.; Ma, S.; Yin, Z.; Huang, Y. A Review on Metal–Organic Framework-Derived Porous Carbon-Based Novel Microwave Absorption Materials. *Nanomicro Lett.* 2021, 13, 56. doi:10.1007/s40820-020-00582-3.
7. Ren, S.; Yu, H.; Wang, L.; Huang, Z.; Lin, T.; Huang, Y.; Yang, J.; Hong, Y.; Liu, J. State of the Art and Prospects in Metal–Organic Framework-Derived Microwave Absorption Materials. *Nanomicro Lett.* 2022, 14, 68. doi:10.1007/s40820-022-00808-6.
8. Liang, C.; Gu, Z.; Zhang, Y.; Ma, Z.; Qiu, H.; Gu, J. Structural Design Strategies of Polymer Matrix Composites for Electromagnetic Interference Shielding: A Review. *Nanomicro. Lett.* 2021, 13, 181. doi:10.1007/s40820-021-00707-2.
9. Cheng, J.; Li, C.; Xiong, Y.; Zhang, H.; Raza, H.; Ullah, S.; Wu, J.; Zheng, G.; Cao, Q.; Zhang, D.; et al. Recent Advances in Design Strategies and Multifunctionality of Flexible Electromagnetic Interference Shielding Materials. *Nanomicro. Lett.* 2022, 14, 80. doi:10.1007/s40820-022-00823-7.
10. Fei, Y.; Liang, M.; Chen, Y.; Zou, H. Sandwich-like Magnetic Graphene Papers Prepared with MOF-Derived Fe₃O₄–C for Absorption-Dominated Electromagnetic Interference Shielding. *Ind. Eng. Chem. Res.* 2020, 59, 154–165. doi:10.1021/acs.iecr.9b04416.
11. Kato, Y.; Horibe, M.; Ata, S.; Yamada, T.; Hata, K. Stretchable Electromagnetic-Interference Shielding Materials Made of a Long Single-Walled Carbon Nanotube–Elastomer Composite. *RSC Adv.* 2017, 7, 10841–10847. doi:10.1039/C6RA25350D.
12. Biswas, S.; Kar, G. P.; Bose, S. Tailor-Made Distribution of Nanoparticles in Blend Structure toward Outstanding Electromagnetic Interference Shielding. *ACS Appl. Mater. Interfaces* 2015, 7, 25448–25463. doi:10.1021/acsami.5b08333.
13. Arief, I.; Biswas, S.; Bose, S. Tuning the Shape Anisotropy and Electromagnetic Screening Ability of Ultrahigh Magnetic Polymer and Surfactant-Capped FeCo Nanorods and Nanocubes in Soft Conducting Composites. *ACS Appl. Mater. Interfaces* 2016, 8, 26285–26297. doi:10.1021/acsami.6b07464.
14. Zhang, C.; Peng, Y.; Song, Y.; Li, J.; Yin, F.; Yuan, Y. Periodic Three-Dimensional Nitrogen-Doped Mesoporous Carbon Spheres Embedded with Co/Co₃O₄ Nanoparticles toward Microwave Absorption. *ACS Appl. Mater. Interfaces* 2020, 12, 24102–24111. doi:10.1021/acsami.0c03105.
15. Li, W.; Qiu, T.; Wang, L.; Ren, S.; Zhang, J.; He, L.; Li, X. Preparation and Electromagnetic Properties of Core/Shell Polystyrene@Polypyrrole@Nickel Composite Microspheres. *ACS Appl. Mater. Interfaces* 2013, 5, 883–891. doi:10.1021/am302551d.
16. Wang, X.-X.; Zheng, Q.; Zheng, Y.-J.; Cao, M.-S. Green EMI Shielding: Dielectric/Magnetic “Genes” and Design Philosophy. *Carbon* 2023, 206, 124–141. doi:10.1016/j.carbon.2023.02.012.
17. Wang, Q.; Niu, B.; Han, Y.; Zheng, Q.; Li, L.; Cao, M. Nature-Inspired 3D Hierarchical Structured “Vine” for Efficient Microwave Attenuation and Electromagnetic Energy Conversion Device. *Chemical Engineering Journal* 2023, 452, 139042. doi:10.1016/j.cej.2022.139042.
18. Wu, Z.; Pei, K.; Xing, L.; Yu, X.; You, W.; Che, R. Enhanced Microwave Absorption Performance from Magnetic Coupling of Magnetic Nanoparticles

- Suspended within Hierarchically Tubular Composite. *Adv. Funct. Mater.* 2019, 29, 1901448. doi:10.1002/adfm.201901448.
19. Wu, F.; Liu, Z.; Xiu, T.; Zhu, B.; Khan, I.; Liu, P.; Zhang, Q.; Zhang, B. Fabrication of Ultralight Helical Porous Carbon Fibers with CNTs-Confined Ni Nanoparticles for Enhanced Microwave Absorption. *Compos. B* 2021, 215, 108814. doi:10.1016/j.compositesb.2021.108814.
 20. Fei, Y.; Wang, X.; Yuan, M.; Liang, M.; Chen, Y.; Zou, H. Co Nanoparticles Encapsulated in Carbon Nanotubes Decorated Carbon Aerogels toward Excellent Microwave Absorption. *Ind. Eng. Chem. Res.* 2022, 61, 1684–1693. doi:10.1021/acs.iecr.1c03585.
 21. Cao, M.-S.; Song, W.-L.; Hou, Z.-L.; Wen, B.; Yuan, J. The Effects of Temperature and Frequency on the Dielectric Properties, Electromagnetic Interference Shielding and Microwave-Absorption of Short Carbon Fiber/Silica Composites. *Carbon* 2010, 48, 788–796. doi:10.1016/j.carbon.2009.10.028.
 22. Gao, X.; Wu, X.; Qiu, J. High Electromagnetic Waves Absorbing Performance of a Multilayer-Like Structure Absorber Containing Activated Carbon Hollow Porous Fibers–Carbon Nanotubes and Fe₃O₄ Nanoparticles. *Adv. Electron. Mater.* 2018, 4, 1700565. doi:10.1002/aelm.201700565.
 23. Wang, X.-Y.; Ma, L.; Zhao, Q.; Hyun, B. G.; Liu, H.; Yu, L.; Wang, J.; Park, C. B. Flexible Poly(Ether-Block-Amide)/Carbon Nanotube Composites for Electromagnetic Interference Shielding. *ACS Appl. Nano Mater.* 2022, 5, 7598–7608. doi:10.1021/acsnm.2c01729.
 24. Fang, Y.-S.; Yuan, J.; Liu, T.-T.; Wang, Q.-Q.; Cao, W.-Q.; Cao, M.-S. Clipping Electron Transport and Polarization Relaxation of Ti₃C₂T_x Based Nanocomposites towards Multifunction. *Carbon* 2023, 201, 371–380. doi:10.1016/j.carbon.2022.09.043.
 25. Wen, B.; Cao, M.-S.; Hou, Z.-L.; Song, W.-L.; Zhang, L.; Lu, M.-M.; Jin, H.-B.; Fang, X.-Y.; Wang, W.-Z.; Yuan, J. Temperature Dependent Microwave Attenuation Behavior for Carbon-Nanotube/Silica Composites. *Carbon* 2013, 65, 124–139. doi:10.1016/j.carbon.2013.07.110.
 26. Ghosh, S. K.; Das, T. K.; Ganguly, S.; Paul, S.; Nath, K.; Katheria, A.; Ghosh, T.; Chowdhury, S. N.; Das, N. C. Carbon Nanotubes and Carbon Nanofibers Based Co-Continuous Thermoplastic Elastomeric Blend Composites for Efficient Microwave Shielding and Thermal Management. *Compos. A* 2022, 161, 107118. doi:10.1016/j.compositesa.2022.107118.
 27. Das, P.; Katheria, A.; Ghosh, S.; Roy, B.; Nayak, J.; Nath, K.; Paul, S.; Das, N. C. Self-Healable and Super-Stretchable Conductive Elastomeric Nanocomposites for Efficient Thermal Management Characteristics and Electromagnetic Interference Shielding. *Synth. Met.* 2023, 294, 117304. doi:10.1016/j.synthmet.2023.117304.
 28. Sang, G.; Wang, C.; Zhao, Y.; He, G.; Zhang, Q.; Yang, M.; Zhao, S.; Xu, P.; Xi, X.; Yang, J.; et al. Ni@CNTs/Al₂O₃ Ceramic Composites with Interfacial Solder Strengthen the Segregated Network for High Toughness and Excellent Electromagnetic Interference Shielding. *ACS Appl. Mater. Interfaces* 2022, 14, 4443–4455. doi:10.1021/acsami.1c21630.
 29. Xiao, X.; Zhu, W.; Tan, Z.; Tian, W.; Guo, Y.; Wang, H.; Fu, J.; Jian, X. Ultra-Small Co/CNTs Nanohybrid from Metal Organic Framework with Highly Efficient Microwave Absorption. *Compos. B* 2018, 152, 316–323. doi:10.1016/j.compositesb.2018.08.109.
 30. Lu, M.-M.; Cao, M.-S.; Chen, Y.-H.; Cao, W.-Q.; Liu, J.; Shi, H.-L.; Zhang, D.-Q.; Wang, W.-Z.; Yuan, J. Multiscale Assembly of Grape-Like Ferroferri Oxide and Carbon Nanotubes: A Smart Absorber Prototype Varying Temperature to Tune Intensities. *ACS Appl. Mater. Interfaces* 2015, 7, 19408–19415. doi:10.1021/acsami.5b05595.
 31. Zou, Y.; Huang, X.; Fan, B.; Liu, Y.; Yue, J. Triple-Layer Structure of Carbon Foam Coated with Carbon Nanotubes and FeNi Alloy for High-Performance Electromagnetic Wave Absorption. *J. Alloys Compd.* 2023, 946, 169404. doi:10.1016/j.jallcom.2023.169404.
 32. Xu, J.; Bian, C.; Sun, J.; Liu, D.; Wang, X.; Xue, Z.; Meng, X.; Wu, H. Heterostructure Tailoring of Carbon Nanotubes Grown on Prismatic NiCo Clusters for High-Efficiency Electromagnetic Absorption. *J. Colloid Interface Sci.* 2023, 634, 185–194. doi:10.1016/j.jcis.2022.12.037.
 33. Yang, L.; Wang, Y.; Lu, Z.; Cheng, R.; Wang, N.; Li, Y. Construction of Multi-Dimensional NiCo/C/CNT/rGO Aerogel by MOF Derivative for Efficient Microwave Absorption. *Carbon* 2023, 205, 411–421. doi:10.1016/j.carbon.2023.01.057.
 34. Hu, J.; Liang, C.; Li, J.; Lin, C.; Liang, Y.; Wang, H.; Li, X.; Wang, Q.; Dong, D. Lewis Acidic Molten Salts Etching Route Driven Construction of Double-Layered MXene-Fe/Carbon Nanotube/Silicone Rubber Composites for High-Performance Microwave Absorption. *Carbon* 2023, 204, 136–146. doi:10.1016/j.carbon.2022.12.050.
 35. Yao, Z.; Xu, S.; Zhang, X.; Yuan, J.; Rong, C.; Xiong, Z.; Zhu, X.; Yu, Y.; Yu, H.; Kang, S.; Kuang, F. CuCo Nanocube/N-Doped Carbon Nanotube Composites for Microwave Absorption. *ACS Appl. Nano Mater.* 2023, 6, 1325–1338. doi:10.1021/acsnm.2c04972.
 36. Kefeni, K. K.; Msagati, T. A. M.; Mamba, B. B. Ferrite Nanoparticles: Synthesis, Characterisation and Applications in Electronic Device. *Mater. Sci. Eng., B* 2017, 215, 37–55. doi:10.1016/j.mseb.2016.11.002.
 37. Shokrollahi, H.; Avazpour, L. Influence of Intrinsic Parameters on the Particle Size of Magnetic Spinel Nanoparticles Synthesized by Wet Chemical Methods. *Particuology* 2016, 26, 32–39. doi:10.1016/j.partic.2015.10.004.
 38. Feng, J.; Hou, Y.; Wang, Y.; Li, L. Synthesis of Hierarchical ZnFe₂O₄@SiO₂@RGO Core–Shell Microspheres for Enhanced Electromagnetic Wave Absorption. *ACS Appl. Mater. Interfaces* 2017, 9, 14103–14111. doi:10.1021/acsami.7b03330.
 39. Lou, Z.; Li, Y.; Han, H.; Ma, H.; Wang, L.; Cai, J.; Yang, L.; Yuan, C.; Zou, J. Synthesis of Porous 3D Fe/C Composites from Waste Wood with Tunable and Excellent Electromagnetic Wave Absorption

- Performance. *ACS Sustainable Chem. Eng.* 2018, 6, 15598–15607. doi:10.1021/acssuschemeng.8b04045.
40. Sankaran, S.; Deshmukh, K.; Ahamed, M. B.; Pasha, S. K. Recent Advances in Electromagnetic Interference Shielding Properties of Metal and Carbon Filler Reinforced Flexible Polymer Composites: A Review. *Compos. A* 2018, 114, 49–71. doi:10.1016/j.compositesa.2018.08.006.
 41. Zhao, B.; Hamidinejad, M.; Wang, S.; Bai, P.; Che, R.; Zhang, R.; Park, C. B. Advances in Electromagnetic Shielding Properties of Composite Foams. *J. Mater. Chem. A* 2021, 9, 8896–8949. doi:10.1039/D1TA00417D.
 42. Sharma, G. K.; James, N. R. Progress in Electrospun Polymer Composite Fibers for Microwave Absorption and Electromagnetic Interference Shielding. *ACS Appl. Electron. Mater.* 2021, 3, 4657–4680. doi:10.1021/acsaem.1c00827.
 43. Kumar, R.; Sahoo, S.; Joanni, E.; Singh, R. K.; Tan, W. K.; Kar, K. K.; Matsuda, A. Recent Progress on Carbon-Based Composite Materials for Microwave Electromagnetic Interference Shielding. *Carbon* 2021, 177, 304–331. doi:10.1016/j.carbon.2021.02.091.
 44. Ghosh, S. K.; Das, T. K.; Ghosh, S.; Remanan, S.; Nath, K.; Das, P.; Das, N. C. Selective Distribution of Conductive Carbonaceous Inclusion in Thermoplastic Elastomer: A Wet Chemical Approach of Promoting Dual Percolation and Inhibiting Radiation Pollution in X-Band. *Compos. Sci. Technol.* 2021, 210, 108800. doi:10.1016/j.compscitech.2021.108800.
 45. Iqbal, A.; Hassan, T.; Gao, Z.; Shahzad, F.; Koo, C. M. MXene-Incorporated 1D/2D Nano-Carbons for Electromagnetic Shielding: A Review. *Carbon* 2023, 203, 542–560. doi:10.1016/j.carbon.2022.11.104.
 46. Zhou, M.; Gu, W.; Wang, G.; Zheng, J.; Pei, C.; Fan, F.; Ji, G. Sustainable Wood-Based Composites for Microwave Absorption and Electromagnetic Interference Shielding. *J. Mater. Chem. A* 2020, 8, 24267–24283. doi:10.1039/D0TA08372K.
 47. Wang, C.; Murugadoss, V.; Kong, J.; He, Z.; Mai, X.; Shao, Q.; Chen, Y.; Guo, L.; Liu, C.; Angaiah, S.; et al. Overview of Carbon Nanostructures and Nanocomposites for Electromagnetic Wave Shielding. *Carbon* 2018, 140, 696–733. doi:10.1016/j.carbon.2018.09.006.
 48. Guan, H.; Wang, Q.; Wu, X.; Pang, J.; Jiang, Z.; Chen, G.; Dong, C.; Wang, L.; Gong, C. Biomass Derived Porous Carbon (BPC) and Their Composites as Lightweight and Efficient Microwave Absorption Materials. *Compos. B* 2021, 207, 108562. doi:10.1016/j.compositesb.2020.108562.
 49. Meng, F.; Wang, H.; Huang, F.; Guo, Y.; Wang, Z.; Hui, D.; Zhou, Z. Graphene-Based Microwave Absorbing Composites: A Review and Prospective. *Compos. B* 2018, 137, 260–277. doi:10.1016/j.compositesb.2017.11.023.
 50. Cao, M.; Han, C.; Wang, X.; Zhang, M.; Zhang, Y.; Shu, J.; Yang, H.; Fang, X.; Yuan, J. Graphene Nanohybrids: Excellent Electromagnetic Properties for the Absorbing and Shielding of Electromagnetic Waves. *J. Mater. Chem. C* 2018, 6, 4586–4602. doi:10.1039/C7TC05869A.
 51. Jiang, D.; Murugadoss, V.; Wang, Y.; Lin, J.; Ding, T.; Wang, Z.; Shao, Q.; Wang, C.; Liu, H.; Lu, N.; et al. Electromagnetic Interference Shielding Polymers and Nanocomposites - A Review. *Polym. Rev.* 2019, 59, 280–337. doi:10.1080/15583724.2018.1546737.
 52. Lyu, L.; Wang, F.; Zhang, X.; Qiao, J.; Liu, C.; Liu, J. CuNi Alloy/Carbon Foam Nanohybrids as High-Performance Electromagnetic Wave Absorbers. *Carbon* 2021, 172, 488–496. doi:10.1016/j.carbon.2020.10.021.
 53. Shukla, V. Review of Electromagnetic Interference Shielding Materials Fabricated by Iron Ingredients. *Nanoscale Adv.* 2019, 1, 1640–1671. doi:10.1039/C9NA00108E.
 54. Wang, L.; Li, X.; Shi, X.; Huang, M.; Li, X.; Zeng, Q.; Che, R. Recent Progress of Microwave Absorption Microspheres by Magnetic–Dielectric Synergy. *Nanoscale* 2021, 13, 2136–2156. doi:10.1039/D0NR06267G.
 55. Quan, B.; Liang, X.; Ji, G.; Cheng, Y.; Liu, W.; Ma, J.; Zhang, Y.; Li, D.; Xu, G. Dielectric Polarization in Electromagnetic Wave Absorption: Review and Perspective. *J. Alloys Compd.* 2017, 728, 1065–1075. doi:10.1016/j.jallcom.2017.09.082.
 56. Charles, A. D.; Rider, A. N.; Brown, S. A.; Wang, C. H. Multifunctional Magneto-Polymer Matrix Composites for Electromagnetic Interference Suppression, Sensors and Actuators. *Prog. Mater. Sci.* 2021, 115, 100705. doi:10.1016/j.pmatsci.2020.100705.
 57. Lv, H.; Liang, X.; Ji, G.; Zhang, H.; Du, Y. Porous Three-Dimensional Flower-like Co/CoO and Its Excellent Electromagnetic Absorption Properties. *ACS Appl. Mater. Interfaces* 2015, 7, 9776–9783. doi:10.1021/acsami.5b01654.
 58. Ibrahim, I. R.; Matori, K. A.; Ismail, I.; Awang, Z.; Rusly, S. N. A.; Nazlan, R.; Mohd Idris, F.; Muhammad Zulkimi, M. M.; Abdullah, N. H.; Mustaffa, M. S.; et al. A Study on Microwave Absorption Properties of Carbon Black and Ni_{0.6}Zn_{0.4}Fe₂O₄ Nanocomposites by Tuning the Matching-Absorbing Layer Structures. *Sci. Rep.* 2020, 10, 3135. doi:10.1038/s41598-020-60107-1.
 59. Bhattacharjee, Y.; Bose, S. Core–Shell Nanomaterials for Microwave Absorption and Electromagnetic Interference Shielding: A Review. *ACS Appl. Nano Mater.* 2021, 4, 949–972. doi:10.1021/acsnm.1c00278.
 60. Xia, L.; Feng, Y.; Zhao, B. Intrinsic Mechanism and Multiphysics Analysis of Electromagnetic Wave Absorbing Materials: New Horizons and Breakthrough. *J. Mater. Sci. Technol.* 2022, 130, 136–156. doi:10.1016/j.jmst.2022.05.010.
 61. Kumar, R.; Sahoo, S.; Joanni, E.; Singh, R. K.; Tan, W. K.; Moshkalev, S. A.; Matsuda, A.; Kar, K. K. Heteroatom Doping of 2D Graphene Materials for Electromagnetic Interference Shielding: A Review of Recent Progress. *Crit. Rev. Solid State Mater. Sci.* 2022, 47, 570–619. doi:10.1080/10408436.2021.1965954.

62. Xu, Z.; Du, Y.; Liu, D.; Wang, Y.; Ma, W.; Wang, Y.; Xu, P.; Han, X. Pea-like Fe/Fe₃C Nanoparticles Embedded in Nitrogen-Doped Carbon Nanotubes with Tunable Dielectric/Magnetic Loss and Efficient Electromagnetic Absorption. *ACS Appl. Mater. Interfaces* 2019, 11, 4268–4277. doi:10.1021/acsami.8b19201.
63. Gupta, S.; Tai, N.-H. Carbon Materials and Their Composites for Electromagnetic Interference Shielding Effectiveness in X-Band. *Carbon* 2019, 152, 159–187. doi:10.1016/j.carbon.2019.06.002.
64. Zhu, L.; Zeng, X.; Chen, M.; Yu, R. Controllable Permittivity in 3D Fe₃O₄/CNTs Network for Remarkable Microwave Absorption Performances. *RSC Adv.* 2017, 7, 26801–26808. doi:10.1039/C7RA04456A.
65. Wu, T.; Liu, Y.; Zeng, X.; Cui, T.; Zhao, Y.; Li, Y.; Tong, G. Facile Hydrothermal Synthesis of Fe₃O₄/C Core-Shell Nanorings for Efficient Low-Frequency Microwave Absorption. *ACS Appl. Mater. Interfaces* 2016, 8, 7370–7380. doi:10.1021/acsami.6b00264.
66. Zeng, X.; Sang, Y.; Xia, G.; Jiang, G.; Xie, N.; Zheng, N.; Cheng, Y.; Yu, R. 3-D Hierarchical Urchin-like Fe₃O₄/CNTs Architectures Enable Efficient Electromagnetic Microwave Absorption. *Mater. Sci. Eng. B* 2022, 281, 115721. doi:10.1016/j.mseb.2022.115721.
67. Yuan, H.; Xu, Y.; Jia, H.; Zhou, S. Superparamagnetic Fe₃O₄/MWCNTs Heterostructures for High Frequency Microwave Absorption. *RSC Adv.* 2016, 6, 67218–67225. doi:10.1039/C6RA11610H.
68. Chen, Y.-H.; Huang, Z.-H.; Lu, M.-M.; Cao, W.-Q.; Yuan, J.; Zhang, D.-Q.; Cao, M.-S. 3D Fe₃O₄ Nanocrystals Decorating Carbon Nanotubes to Tune Electromagnetic Properties and Enhance Microwave Absorption Capacity. *J. Mater. Chem. A* 2015, 3, 12621–12625. doi:10.1039/C5TA02782A.
69. Wang, Z.; Wu, L.; Zhou, J.; Cai, W.; Shen, B.; Jiang, Z. Magnetite Nanocrystals on Multiwalled Carbon Nanotubes as a Synergistic Microwave Absorber. *J. Phys. Chem. C* 2013, 117, 5446–5452. doi:10.1021/jp4000544.
70. Hekmatara, H.; Seifi, M.; Forooraghi, K.; Mirzaee, S. Synthesis and Microwave Absorption Characterization of SiO₂ Coated Fe₃O₄/MWCNT Composites. *Phys. Chem. Chem. Phys.* 2014, 16, 24069–24075. doi:10.1039/C4CP03208J.
71. Yin, P.; Wu, G.; Tang, Y.; Liu, S.; Zhang, Y.; Bu, G.; Dai, J.; Zhao, Y.; Liu, Y. Structure Regulation in N-Doping Biconical Carbon Frame Decorated with CoFe₂O₄ and (Fe,Ni) for Broadband Microwave Absorption. *Chem. Eng. J.* 2022, 446, 136975. doi:10.1016/j.cej.2022.136975.
72. Yue, L.; Zhang, S.; Zhao, H.; Feng, Y.; Wang, M.; An, L.; Zhang, X.; Mi, J. One-Pot Synthesis CoFe₂O₄/CNTs Composite for Asymmetric Supercapacitor Electrode. *Solid State Ion* 2019, 329, 15–24. doi:10.1016/j.ssi.2018.11.006.
73. Li, X.; Yin, X.; Han, M.; Song, C.; Xu, H.; Hou, Z.; Zhang, L.; Cheng, L. Ti₃C₂ MXenes Modified with in Situ Grown Carbon Nanotubes for Enhanced Electromagnetic Wave Absorption Properties. *J. Mater. Chem. C* 2017, 5, 4068–4074. doi:10.1039/C6TC05226F.
74. Ashfaq, M. Z.; Ashfaq, A.; Majeed, M. K.; Saleem, A.; Wang, S.; Ahmad, M.; Hussain, M. M.; Zhang, Y.; Gong, H. Confined Tailoring of CoFe₂O₄/MWCNTs Hybrid-Architectures to Tune Electromagnetic Parameters and Microwave Absorption with Broadened Bandwidth. *Ceram. Int.* 2022, 48, 9569–9578. doi:10.1016/j.ceramint.2021.12.155.
75. Quan, B.; Xu, G.; Li, D.; Liu, W.; Ji, G.; Du, Y. Incorporation of Dielectric Constituents to Construct Ternary Heterojunction Structures for High-Efficiency Electromagnetic Response. *J. Colloid Interface Sci.* 2017, 498, 161–169. doi:10.1016/j.jcis.2017.03.049.
76. Liu, H.; Zhang, M.; Hu, K.; Kong, X.; Li, Q.; Liu, Q. High-Efficiency Microwave Absorption Performance of Cobalt Ferrite Microspheres/Multi-Walled Carbon Nanotube Composites. *J. Mater. Sci.: Mater. Electron.* 2021, 32, 26021–26033. doi:10.1007/s10854-021-05877-8.
77. Yuan, Y.; Wei, S.; Liang, Y.; Wang, B.; Wang, Y.; Xin, W.; Wang, X.; Zhang, Y. Solvothermal Assisted Synthesis of CoFe₂O₄/CNTs Nanocomposite and Their Enhanced Microwave Absorbing Properties. *J. Alloys Compd.* 2021, 867, 159040. doi:10.1016/j.jallcom.2021.159040.
78. Huang, D.; Dai, J.; Wang, Q.; Liu, H.; Li, Z. MWCNTs Wrapped in Hollow with Open Holes of CoFe₂O₄ as High-Performance Electromagnetic Wave Absorbers. *J. Alloys Compd.* 2023, 944, 169194. doi:10.1016/j.jallcom.2023.169194.
79. Soomro, S. A.; Gul, I. H.; Khan, M. Z.; Naseer, H.; Khan, A. N. Dielectric Properties Evaluation of NiFe₂O₄/MWCNTs Nanohybrid for Microwave Applications Prepared via Novel One Step Synthesis. *Ceram. Int.* 2017, 43, 4090–4095. doi:10.1016/j.ceramint.2016.12.002.
80. Guo, L.; He, Y.; Chen, D.; Du, B.; Cao, W.; Lv, Y.; Ding, Z. Hydrothermal Synthesis and Microwave Absorption Properties of Nickel Ferrite/Multiwalled Carbon Nanotubes Composites. *Coatings* 2021, 11, 534. doi:10.3390/coatings11050534.
81. Zuo, Y.; Su, X.; Li, X.; Yao, Z.; Yu, T.; Zhou, J.; Li, J.; Lu, J.; Ding, J. Multimaterial 3D-Printing of Graphene/Li_{0.35}Zn_{0.3}Fe_{2.35}O₄ and Graphene/Carbonyl Iron Composites with Superior Microwave Absorption Properties and Adjustable Bandwidth. *Carbon* 2020, 167, 62–74. doi:10.1016/j.carbon.2020.05.071.
82. Rostami, M.; Ara, M. H. M. The Dielectric, Magnetic and Microwave Absorption Properties of Cu-Substituted Mg-Ni Spinel ferrite-MWCNT Nanocomposites. *Ceram. Int.* 2019, 45, 7606–7613. doi:10.1016/j.ceramint.2019.01.056.
83. Chen, N.; Zhou, J.; Yao, Z.; Lei, Y.; Tan, R.; Zuo, Y.; Zheng, W.; Jiao, Z. Fabrication of Nd-Doped Ni-Zn Ferrite/Multi-Walled Carbon Nanotubes Composites with Effective Microwave Absorption Properties. *Ceram. Int.* 2021, 47, 10545–10554. doi:10.1016/j.ceramint.2020.11.137.
84. Mustaffa, M. S.; Azis, R. S.; Abdullah, N. H.; Ismail, I.; Ibrahim, I. R. An Investigation of Microstructural,

- Magnetic and Microwave Absorption Properties of Multiwalled Carbon Nanotubes/Ni_{0.5}Zn_{0.5}Fe₂O₄. *Sci. Rep.* 2019, 9, 15523. doi:10.1038/s41598-019-52233-2.
85. Dalal, M.; Mallick, A.; Greneche, J.-M.; Das, D.; Chakrabarti, P. K. Correlation of Cation Distribution with the Hyperfine and Magnetic Behaviour of Ni_{0.3}Zn_{0.4}Co_{0.2}Cu_{0.1}Fe₂O₄ Nanoparticles and Their Microwave Absorption Properties When Encapsulated in Multi-Walled Carbon Nanotubes. *J. Phys. Condens. Matter* 2017, 29, 085803. doi:10.1088/1361-648X/aa5169.
 86. Chahar, M.; Dabas, S.; Thakur, O. P. Enhanced Electromagnetic Shielding Effectiveness of MWCNT/Zinc-Doped Nickel Ferrite Nanocomposites. *Ceram. Int.* 2022, 48, 5352–5360. doi:10.1016/j.ceramint.2021.11.078.
 87. Gao, Y.; Wang, Z. Microwave Absorption and Electromagnetic Interference Shielding Properties of Li-Zn Ferrite-Carbon Nanotubes Composite. *J. Magn. Magn. Mater.* 2021, 528, 167808. doi:10.1016/j.jmmm.2021.167808.
 88. Zhou, Y.; Zhao, X.; Liu, F.; Chi, W.; Yao, J.; Chen, G. Facile One-Pot Solvothermal Synthesis of the RGO/MWCNT/Fe₃O₄ Hybrids for Microwave Absorption. *ACS Omega.* 2020, 5, 2899–2909. doi:10.1021/acsomega.9b03740.
 89. Shu, R.; Zhang, G.; Zhang, J.; Wang, X.; Wang, M.; Gan, Y.; Shi, J.; He, J. Fabrication of Reduced Graphene Oxide/Multi-Walled Carbon Nanotubes/Zinc Ferrite Hybrid Composites as High-Performance Microwave Absorbers. *J. Alloys Compd.* 2018, 736, 1–11. doi:10.1016/j.jallcom.2017.11.084.
 90. Zhou, J.; Tao, H.; Xia, L.; Zhao, H.; Wang, Y.; Zhan, Y.; Yuan, B. An Innovative Ternary Composite Paper of Graphene and Fe₃O₄ Decorated Multi-Walled Carbon Nanotube for Ultra-Efficient Electromagnetic Interference Shielding and Fire-Resistant Properties. *Compos. Commun.* 2022, 32, 101181. doi:10.1016/j.coco.2022.101181.
 91. Zhang, K.; Gao, X.; Zhang, Q.; Chen, H.; Chen, X. Fe₃O₄ Nanoparticles Decorated MWCNTs @ C Ferrite Nanocomposites and Their Enhanced Microwave Absorption Properties. *J. Magn. Magn. Mater.* 2018, 452, 55–63. doi:10.1016/j.jmmm.2017.12.039.
 92. Yin, P.; Zhang, L.; Wu, H.; Feng, X.; Wang, J.; Rao, H.; Wang, Y.; Dai, J.; Tang, Y. Two-Step Solvothermal Synthesis of (Zn_{0.5}Co_{0.5}Fe₂O₄/Mn_{0.5}Ni_{0.5}Fe₂O₄)@C-MWCNTs Hybrid with Enhanced Low Frequency Microwave Absorbing Performance. *Nanomaterials* 2019, 9, 1601. doi:10.3390/nano9111601.
 93. Ling, Z.; Ren, C. E.; Zhao, M.-Q.; Yang, J.; Giammarco, J. M.; Qiu, J.; Barsoum, M. W.; Gogotsi, Y. Flexible and Conductive MXene Films and Nanocomposites with High Capacitance. *Proc. Natl. Acad. Sci. U. S. A.* 2014, 111, 16676–16681. doi:10.1073/pnas.1414215111.
 94. Liu, H.; Wang, Z.; Yang, Y.; Wu, S.; Wang, C.; You, C.; Tian, N. Thermally Conductive MWCNTs/Fe₃O₄/Ti₃C₂T_x MXene Multi-Layer Films for Broadband Electromagnetic Interference Shielding. *J. Mater. Sci. Technol.* 2022, 130, 75–85. doi:10.1016/j.jmst.2022.05.009.
 95. Kumar, S.; Kumar, P.; Singh, N.; Kansal, M. K.; Kumar, A.; Verma, V. Highly Efficient and Sustainable MXene Based Heterostructure Composites Filled with Ferrites and MWCNTs to Mitigate the Radiation Interference in X-Band Frequency Region. *Mater. Sci. Eng. B* 2022, 282, 115798. doi:10.1016/j.mseb.2022.115798.
 96. Li, Z.; Li, X.; Zong, Y.; Tan, G.; Sun, Y.; Lan, Y.; He, M.; Ren, Z.; Zheng, X. Solvothermal Synthesis of Nitrogen-Doped Graphene Decorated by Superparamagnetic Fe₃O₄ Nanoparticles and Their Applications as Enhanced Synergistic Microwave Absorbers. *Carbon* 2017, 115, 493–502. doi:10.1016/j.carbon.2017.01.036.
 97. Feng, J.; Zong, Y.; Sun, Y.; Zhang, Y.; Yang, X.; Long, G.; Wang, Y.; Li, X.; Zheng, X. Optimization of Porous FeNi₃/N-GN Composites with Superior Microwave Absorption Performance. *Chem. Eng. J.* 2018, 345, 441–451. doi:10.1016/j.cej.2018.04.006.
 98. Wang, X.; Ma, T.; Shu, J.; Cao, M. Confinedly Tailoring Fe₃O₄ clusters-NG to Tune Electromagnetic Parameters and Microwave Absorption with Broadened Bandwidth. *Chem. Eng. J.* 2018, 332, 321–330. doi:10.1016/j.cej.2017.09.101.
 99. Shu, R.; Zhang, J.; Wu, Y.; Wan, Z.; Zheng, M. Facile Design of Nitrogen-Doped Reduced Graphene Oxide/Zinc Ferrite Hybrid Nanocomposites with Excellent Microwave Absorption in the X-Band. *Mater. Lett.* 2019, 255, 126549. doi:10.1016/j.matlet.2019.126549.
 100. Shu, R.; Wu, Y.; Li, Z.; Zhang, J.; Wan, Z.; Liu, Y.; Zheng, M. Facile Synthesis of Cobalt-Zinc Ferrite Microspheres Decorated Nitrogen-Doped Multi-Walled Carbon Nanotubes Hybrid Composites with Excellent Microwave Absorption in the X-Band. *Compos. Sci. Technol.* 2019, 184, 107839. doi:10.1016/j.compscitech.2019.107839.
 101. Li, N.; Huang, G.-W.; Li, Y.-Q.; Xiao, H.-M.; Feng, Q.-P.; Hu, N.; Fu, S.-Y. Enhanced Microwave Absorption Performance of Coated Carbon Nanotubes by Optimizing the Fe₃O₄ Nanocoating Structure. *ACS Appl. Mater. Interfaces* 2017, 9, 2973–2983. doi:10.1021/acsami.6b13142.
 102. Pang, H.; Sahu, R. P.; Liu, J.; Fu, Y.; Huang, L.; Duan, Y.; Puri, I. K. Facile Synthesis of a Hierarchical Multi-Layered CNT-NiFe₂O₄@MnO₂ Composite with Enhanced Microwave Absorbing Performance. *Appl. Surf. Sci.* 2022, 581, 152363. doi:10.1016/j.apsusc.2021.152363.
 103. Wang, X.; Wei, S.; Yuan, Y.; Li, R.; Wang, Y.; Liang, Y.; Wang, B.; Dong, C. Effect of Copper Sulfide Nanosphere Shell on Microstructure and Microwave Absorption Properties of Cobalt Ferrite/Carbon Nanotube Composites. *J. Alloys Compd.* 2022, 909, 164676. doi:10.1016/j.jallcom.2022.164676.
 104. Yadav, R. S.; Pötschke, P.; Pionteck, J.; Krause, B.; Kuřitka, I.; Vilcakova, J.; Skoda, D.; Urbánek, P.; Machovsky, M.; Masař, M.; et al. High-Performance, Lightweight, and Flexible Thermoplastic Polyurethane Nanocomposites with Zn²⁺-Substituted CoFe₂O₄ Nanoparticles and Reduced Graphene Oxide as Shielding Materials against Electromagnetic Pollution.

- ACS Omega 2021, 6, 28098–28118. doi:10.1021/acso-mega.1c04192.
105. Yadav, R. S.; Kuřitka, I.; Vilcakova, J.; Machovsky, M.; Skoda, D.; Urbánek, P.; Masař, M.; Jurča, M.; Urbánek, M.; Kalina, L.; et al. NiFe₂O₄ Nanoparticles Synthesized by Dextrin from Corn-Mediated Sol – Gel Combustion Method and Its Polypropylene Nanocomposites Engineered with Reduced Graphene Oxide for the Reduction of Electromagnetic Pollution. *ACS Omega* 2019, 4, 22069–22081. doi:10.1021/acso-mega.9b03191.
106. Yadav, R. S.; Kuřitka, I.; Vilcakova, J.; Skoda, D.; Urbánek, P.; Machovsky, M.; Masař, M.; Kalina, L.; Havlica, J. Lightweight NiFe₂O₄-Reduced Graphene Oxide-Elastomer Nanocomposite Flexible Sheet for Electromagnetic Interference Shielding Application. *Compos. B* 2019, 166, 95–111. doi:10.1016/j.compositesb.2018.11.069.
107. Biswas, S.; Panja, S. S.; Bose, S. Physical Insight into the Mechanism of Electromagnetic Shielding in Polymer Nanocomposites Containing Multiwalled Carbon Nanotubes and Inverse-Spinel Ferrites. *J. Phys. Chem. C* 2018, 122, 19425–19437. doi:10.1021/acs.jpcc.8b05867.
108. Chen, X.; Yang, M.; Zhao, X.; Hu, D.; Liu, W.; Ma, W. Tailoring Superhydrophobic PDMS/CeFe₂O₄/MWCNTs Nanocomposites with Conductive Network for Highly Efficient Microwave Absorption. *Chem. Eng. J.* 2022, 432, 134226. doi:10.1016/j.cej.2021.134226.
109. Pawar, S. P.; Gandhi, M.; Saraf, C.; Bose, S. Polycarbonate Composites Containing Carbon Encapsulated “Brick-Like” Fe₃O₄ Nanoparticles as Efficient Microwave Absorbers with a Large Bandwidth. *ChemistrySelect* 2016, 1, 3829–3838. doi:10.1002/slct.201600931.
110. Luo, J.; Wang, Y.; Qu, Z.; Wang, W.; Yu, D. Lightweight and Robust Cobalt Ferrite/Carbon Nanotubes/Waterborne Polyurethane Hybrid Aerogels for Efficient Microwave Absorption and Thermal Insulation. *J. Mater. Chem. C* 2021, 9, 12201–12212. doi:10.1039/D1TC02427B.
111. Li, Z.; Feng, D.; Li, B.; Xie, D.; Mei, Y. FDM Printed MXene/MnFe₂O₄/MWCNTs Reinforced TPU Composites with 3D Voronoi Structure for Sensor and Electromagnetic Shielding Applications. *Compos. Sci. Technol.* 2023, 231, 109803. doi:10.1016/j.compscitech.2022.109803.
112. Zhang, X.-P.; Jia, L.-C.; Zhang, G.; Yan, D.-X.; Li, Z.-M. A Highly Efficient and Heat Resistant Electromagnetic Interference Shielding Carbon Nanotube/Poly(Phenylene Sulfide) Composite via Sinter Molding. *J. Mater. Chem. C* 2018, 6, 10760–10766. DOI. doi:10.1039/C8TC03493A
113. Menon, A. V.; Madras, G.; Bose, S. Mussel-Inspired Self-Healing Polyurethane with “Flower-like” Magnetic MoS₂ as Efficient Microwave Absorbers. *ACS Appl. Polym. Mater.* 2019, 1, 2417–2429. doi:10.1021/acsapm.9b00538.
114. Zeng, J.; Zhang, S.; Xue, J.; Dai, H.; Xia, L.; Cai, W.; Tang, Y.; Xu, C. Enhanced Dielectric Loss and Magnetic Loss Properties of Copper Oxide-Nanowire-Covered Carbon Fiber Composites by Porous Nickel Film. *Front. Mater.* 2020, 7, 123. doi:10.3389/fmats.2020.00123.
115. Liu, X.; Feng, C.; Or, S. W.; Sun, Y.; Jin, C.; Li, W.; Lv, Y. Investigation on Microwave Absorption Properties of CuO/Cu₂O-Coated Ni Nanocapsules as Wide-Band Microwave Absorbers. *RSC Adv.* 2013, 3, 14590–14594. doi:10.1039/C3RA40937F.
116. Afzali, S.; Hekmatara, S.; Seyed, S. H.; Yazdi, J.; Hosseini, S. M. B. M. Tuned MWCNT/CuO/Fe₃O₄/Polyaniline Nanocomposites with Exceptional Microwave Attenuation and a Broad Frequency Band. *Sci. Rep.* 2022, 12, 9590. doi:10.1038/s41598-022-13210-4.
117. Zheng, J.; Hanshe, M.; Sun, Z.; Chen, Y.; Jiang, S.; Zhang, Y.; Cao, Y.; Li, X.; Shiju, E. From Waste to Wealth: Crumb Rubber@Carbon Nanotube/Fe₃O₄ Composites towards Highly Effective Electromagnetic Microwave Absorption with Wide Bandwidth. *Diam. Relat. Mater.* 2022, 126, 109089. doi:10.1016/j.diamond.2022.109089.